Complex Nonlinear Waves in Autonomous CNNs Having Two Layers of Memristor Couplings

Makoto Itoh

1-19-20-203, Arae, Jonan-ku,
Fukuoka, 814-0101 JAPAN
Email: itoh-makoto@jcom.home.ne.jp

Abstract

In this paper, we study the nonlinear waves in autonomous cellular neural networks (CNNs) having *double layers* of memristor coupling, by using the *homotopy method*. They can exhibit many interesting nonlinear waves, which are quite different from those in the *single-layer* autonomous CNNs. That is, the autonomous CNNs with *double layers* of memristor coupling can exhibit more complex nonlinear waves and more interesting bifurcation phenomena than those in the *single layer* autonomous CNNs. The above complex behaviors seem to be generated by the interaction with the two nonlinear waves, which are caused by the first layer and the second layer. The most remarkable point in this paper is that the autonomous CNNs with double layers can exhibit complex *deformation behaviors* of the nonlinear waves, due to the changes in the homotopy parameter. That is, we can generate many complex nonlinear waves by adjusting the homotopy parameter, and thereby we can control the complexity of the nonlinear waves. Furthermore, some autonomous CNNs exhibit the sensitive dependence on the homotopy parameter. That is, a small change in the homotopy parameter can result in large differences in a later state. Thus the homotopy method gives a *new approach* to the analysis of the complex nonlinear waves in the autonomous CNNs with double layers.

Keywords

memristor; CNN; homotopy method; nonlinear wave; two layers; memristor grid; synchronous parallel model; complex nonlinear wave; bifurcation phenomenon; sensitive dependence; Lotka-Volterra equations; Van der Pol oscillator; Chua circuit; Rössler equations; Brusselator equations.

1 Introduction

The autonomous CNNs having a *single* layer of memristor coupling can exhibit interesting and complex nonlinear waves. Furthermore, some autonomous CNN can exhibit various kinds of nonlinear waves by changing the initial conditions, or by changing the characteristic curve of the nonlinear resistor [1]. In this paper, we study the nonlinear waves and their bifurcation phenomena in autonomous cellular neural networks having *two layers* of memristor coupling.

If the CNN cell has *dual* synaptic-inputs, then we can easily build the two layers of memristor coupling by connecting dual synaptic-input CNN cells to each node of two layers, which consist of the memristor grids. However, if the CNN cell has only one synaptic-input, that is, it does not have the second synaptic-input (such as the memristor circuit with a single synaptic-input CNN cell in [1]), then we have to realize the second layer by using the CNN cell dynamics, which is coupled to its neighbors via the state equation.

It is easy to imagine that if the autonomous CNN has the *double-layers*, then it would exhibit different nonlinear waves from those for the *single-layer* autonomous CNN. Thus, in order to observe the above difference, we continuously deform the first-layer autonomous CNN equations into the second-layer autonomous

CNN equations using the *homotopy method*.[1] By this method, the nonlinear waves in the former CNN can be deformed into the nonlinear waves in the latter CNN, and we can also observe the complex bifurcation phenomena of the nonlinear waves.

In this paper, we show by computer simulations that the autonomous CNNs with the *double layers* can exhibit more complex nonlinear waves[2] than those in the autonomous CNNs with the *single layer*, and they can also exhibit interesting bifurcation phenomena. That is, the double-layer autonomous CNNs can exhibit many interesting nonlinear waves, which are quite different from those in the single-layer autonomous CNNs. These behaviors seem to be generated by the interaction with the two nonlinear waves, which are caused by the first layer and the second layer. The most remarkable point in this paper is that the autonomous CNNs with double layers of memristor coupling can exhibit complex *deformation behaviors* of the nonlinear waves, due to the changes in the homotopy parameter. That is, we can generate many complex nonlinear waves by adjusting the homotopy parameter, and thereby we can control the complexity of the nonlinear waves. Furthermore, some autonomous CNNs exhibit the sensitive dependence on the homotopy parameter. That is, a small change in the homotopy parameter can result in large differences in a later state. Thus the homotopy method gives a *new approach* to the analysis of the complex nonlinear waves in the autonomous CNNs with double layers.

2 Autonomous CNNs Having Two Layers of Memristor Couplings

Consider the *autonomous* CNNs containing $N \times M$ cells shown in Fig. 1, which are formed by connecting *dual synaptic-input CNN cells* (colored in red) to each node of two layers. In this figure, the first layer consists of brown wires and pink memristors, and the second layer consists of blue wires and yellow memristors. We next show the example of the autonomous CNN having two layers of memristor couplings.
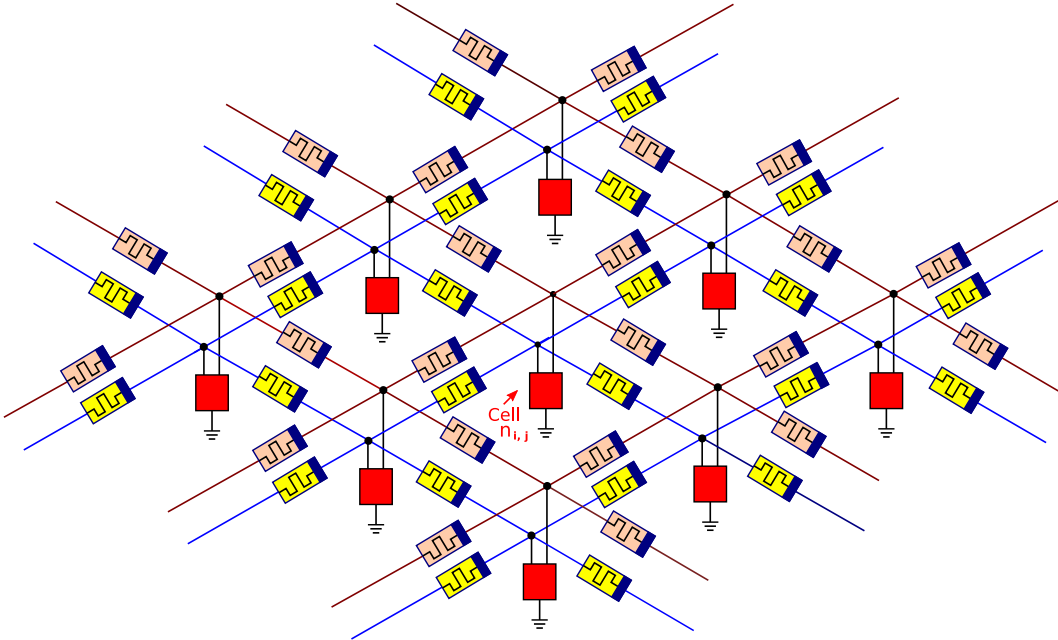

Figure 1: Autonomous CNN formed by connecting dual synaptic-input CNN cells (colored in red) to each node of the first and the second layers, which consist of the memristor grids. The first layer consists of brown wires and pink memristors, and the second layer consists of blue wires and yellow memristors.

---

[1]Two mathematical objects are said to be homotopic if one can be continuously deformed into the other.
[2]In this paper, the term "nonlinear waves" will be used, which can be target (concentric) waves, spiral waves, scroll waves, or chaotic waves, etc. [2]
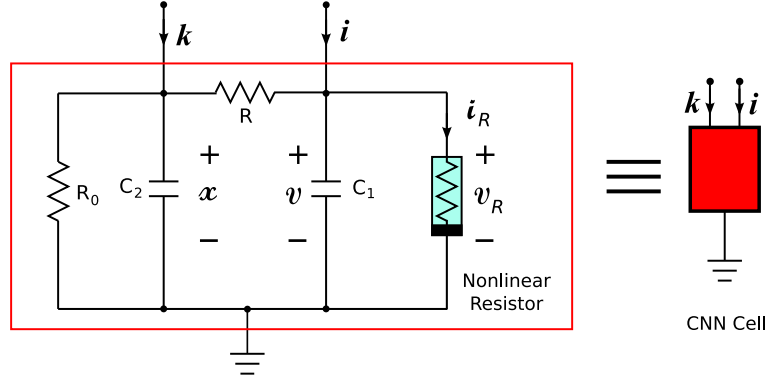
Figure 2: Circuit model for the Van der Pol equations. This circuit contains five circuit elements: a passive capacitor C_1, an active capacitor C_2, an active linear resistor R, and a passive linear resistor R_0, and a nonlinear resistor. The symbols i and k denote the synaptic input currents. The $v - i$ characteristic of the nonlinear resistor is given by $i_R = f(v_R) = \dfrac{v_R{}^3}{3}$. The circuit parameters are given by $C_1 = 1$, $C_2 = -1$, and $R = -1$, and $R_0 = 1$.

2.1 Autonomous Van der Pol CNN

Consider the circuit in Fig. 2 (see [2] for more details). The dynamics of this circuit is given by

$$\left.\begin{array}{rcl} C_1 \dfrac{dv}{dt} & = & \dfrac{x - v}{R} - f(v) + i, \\[2ex] C_2 \dfrac{dx}{dt} & = & -\dfrac{x - v}{R} - \dfrac{x}{R_0} + k, \end{array}\right\} \tag{1}$$

where v and x denote the voltage across the capacitor C_1 and the capacitor C_2, respectively, i and k denote the synaptic input currents. The parameters in Eq. (1) satisfy

$$C_1 = 1,\ C_2 = -1,\ R = -1,\ R_0 = 1. \tag{2}$$

and the $v - i$ characteristic of the nonlinear resistor is given by

$$i_R = f(v_R) \triangleq \dfrac{v_R{}^3}{3}, \tag{3}$$

where $v = v_R$. If we substitute Eqs. (2) and (3) into Eq. (1), the we obtain

$$\left.\begin{array}{rcl} \dfrac{dv}{dt} & = & x - \dfrac{v^3}{3} + v + i, \\[2ex] -\dfrac{dx}{dt} & = & v + k, \end{array}\right\} \tag{4}$$

which is equivalent to the Van der Pol equations, and note that the coefficient of $\dfrac{dx}{dt}$ is *minus* 1.

Assume that the CNN cell is defined by Eq. (4). Then the dynamics of the *double-layer* autonomous CNN in Fig. 1 is given by

$$
\begin{aligned}
\frac{dv_{i,j}}{dt} &= x_{i,j} - f(v_{i,j}) + i_{i,j} = x_{i,j} - \frac{v_{i,j}{}^3}{3} + v_{i,j} + i_{i,j}, \\
-\frac{dx_{i,j}}{dt} &= v_{i,j} + k_{i,j}, \\
\frac{d\varphi_{i,j}}{dt} &= v_{i,j}, \\
\frac{d\psi_{i,j}}{dt} &= x_{i,j},
\end{aligned}
\right\}
\tag{5}
$$

where $i = 1, 2, \cdots, N$, $j = 1, 2, \cdots, M$, the nonlinear function $f(v_{i,j})$ is given by

$$
f(v_{i,j}) = \frac{v_{i,j}{}^3}{3},
\tag{6}
$$

and the six state variables of the CNN cell $n_{i,j}$ are explained as follow:

- $v_{i,j}$ is the voltage across the capacitor C_1 in the CNN cell.
- $i_{i,j}$ is the current through the CNN cell from the first layer.
- $k_{i,j}$ is the current through the CNN cell from the second layer.
- $x_{i,j}$ is the voltage across the capacitor C_2 in the CNN cell.
- $\varphi_{i,j}$ is the flux of the capacitor C_1 in the CNN cell.
- $\psi_{i,j}$ is the flux of the capacitor C_2 in the CNN cell.

The current $i_{i,j}$ and $i_{k,j}$ is given by

$$
\begin{aligned}
i_{i,j} &= W_g(\varphi_{i-1,j} - \varphi_{i,j})(v_{i-1,j} - v_{i,j}) - W_g(\varphi_{i,j} - \varphi_{i+1,j})(v_{i,j} - v_{i+1,j}) \\
&\quad + W_g(\varphi_{i,j-1} - \varphi_{i,j})(v_{i,j-1} - v_{i,j}) - W_g(\varphi_{i,j} - \varphi_{i,j+1})(v_{i,j} - v_{i,j+1}), \\
k_{i,j} &= W_h(\psi_{i-1,j} - \psi_{i,j})(x_{i-1,j} - x_{i,j}) - W_h(\psi_{i,j} - \psi_{i+1,j})(x_{i,j} - x_{i+1,j}) \\
&\quad + W_h(\psi_{i,j-1} - \psi_{i,j})(x_{i,j-1} - x_{i,j}) - W_h(\psi_{i,j} - \psi_{i,j+1})(x_{i,j} - x_{i,j+1}),
\end{aligned}
\tag{7}
$$

where $W_g(\varphi_g)$ and $W_h(\psi_h)$ denote the small-signal memductances of the voltage-controlled *ideal* memristors consisting the first layer and the second layer, respectively. The terminal current i_g and voltage v_g of the memristors in the *first* layer are described by

$$
i_g = W_g(\varphi_g)\, v_g,
\tag{8}
$$

where φ_g is the flux of the memristor in the *first* layer, which satisfies $\dfrac{d\varphi_g}{dt} = v_g$ and $\varphi_g(0) = 0$. Assume that $W_g(\varphi_g)$ is given by a piecewise-linear function of the form:

$$
\begin{aligned}
W_g(\varphi_g) &= \mathfrak{s}\big[\,|\varphi_g| - 0.5\,\big] + 2\,\mathfrak{s}\big[\,|\varphi_g| - 10\,\big] \\
&= \begin{cases}
0 & \text{for} \quad |\varphi_g| < 0.5, \\
1 & \text{for} \quad 0.5 \le |\varphi_g| < 10, \\
3 & \text{for} \quad |\varphi_g| \ge 10,
\end{cases}
\end{aligned}
\tag{9}
$$

where $\mathfrak{s}[\,z\,]$ denotes the *unit step* function, which is equal to 0 for $z < 0$ and 1 for $z \ge 0$. Then the memristors in the *first* layer are *passive*, since the instantaneous power $p_g(t)$ satisfies

$$
p_g(t) = i_g(t)\, v_g(t) = W_g(\varphi_g(t))\, v_g(t)^2 \ge 0.
\tag{10}
$$

Similarly, the terminal current i_h and voltage v_h of the memristors in the *second* layer are described by

$$
i_h = W_h(\psi_h)\, v_h,
\tag{11}
$$

4

where ψ_h is the flux of the memristor in the *second* layer, which satisfies $\dfrac{d\psi_h}{dt} = v_h$ and $\psi_h(0) = 0$. Assume that $W_h(\psi_h)$ given by

$$
\begin{aligned}
W_h(\psi_h) \quad &\triangleq \quad -0.05\,W_g(\psi_h) = -0.05\,\mathfrak{s}\big[\,|\,\psi_h\,|-0.5\,\big] - 0.1\,\mathfrak{s}\big[\,|\,\psi_h\,|-10\,\big] \\[4pt]
&= \quad \left\{
\begin{array}{rl}
0 & \text{for} \quad |\psi_h| < 0.5, \\[4pt]
-0.05 & \text{for} \quad 0.5 \le |\psi_h| < 10, \\[4pt]
-0.15 & \text{for} \quad |\varphi_h| \ge 10.
\end{array}
\right.
\end{aligned}
\tag{12}
$$

Then the memristors in the *second* layer are *not passive*, that is, *locally active*, since the instantaneous power $p(t)$ satisfies

$$
p_h(t) = i_h(t)\,v_h(t) = W_h(\psi_h(t))\,v_h(t)^2 < 0,
\tag{13}
$$

for $0.5 < |\psi_h(t)|$ and $v_h(t) \neq 0$. Note that we have to use the *locally active* memristors in the second layer, since an overflow occurs in the numerical integration process when they are passive. It is due to the reason that the Van der Pol equations are realized by using the active capacitor C_2. That is, the capacitance C_2 has the negative value (that is, $C_2 = -1$).

We next study the behavior of the CNN cell $n_{i,j}$ when the time t is sufficiently small and $\varphi_{i,j}(0) = \psi_{i,j}(0) = 0$. If we recall that $W_g(\varphi_g) = 0$ for $|\varphi_g| < 0.5$ and $W_h(\psi_h) = 0$ for $|\psi_h| < 0.5$, then the currents $i_{i,j}(t)$ and $k_{i,j}(t)$ in the CNN cell $n_{i,j}$ are equal to zero, and individual cells are disconnected from their neighbors at first. That is, they independently operate without interaction at first. However, they interact each other when the currents $i_{i,j}(t)$ and $k_{i,j}(t)$ become non-zero as the time t increases (see [1] for more details).

Let us next introduce the new parameter λ, which can continuously deform the *first-layer* autonomous Van der Pol CNN equations into the *second-layer* autonomous Van der Pol CNN equations:

$$
\left.
\begin{aligned}
\frac{dv_{i,j}}{dt} &= x_{i,j} + v_{i,j} - f(v_{i,j}) + i_{i,j} = x_{i,j} - \frac{v_{i,j}{}^3}{3} + v_{i,j} + \lambda\,i_{i,j}, \\[6pt]
-\frac{dx_{i,j}}{dt} &= v_{i,j} + (1-\lambda)\,k_{i,j}, \\[6pt]
\frac{d\varphi_{i,j}}{dt} &= v_{i,j}, \\[6pt]
\frac{d\psi_{i,j}}{dt} &= x_{i,j},
\end{aligned}
\right\}
\tag{14}
$$

where $0 \le \lambda \le 1$. The homotopy parameter λ deforms Eq. (14) as follow:

- Equation (14) for $\lambda = 0$ is the *single-layer* autonomous Van der Pol CNN equations (*second-layer only*).

- Equation (14) for $\lambda = 1$ is the *single-layer* autonomous Van der Pol CNN equations (*first-layer only*).

- Equation (14) for $0 < \lambda < 1$ is the *double-layer* Van der Pol CNN equations (*both first- and second-layers*).

Thus, we obtain the following table:

Table 1: Parameter dependence of two layers

Parameter value	Layer type	Which layer?
$\lambda = 0$	single-layer	second-layer-only
$\lambda \approx 0$	*nearly* single-layer	*nearly* second-layer-only
$0 < \lambda < 1$	double-layer	*both* first- and second-layers
$\lambda \approx 1$	*nearly* single-layer	*nearly* first-layer-only
$\lambda = 1$	single-layer	first-layer-only

Since Eq. (14) has the homotopy parameter λ, we have to modify the memductances $W_g(\varphi_g)$ in Eq. (9) and $W_h(\psi_h)$ in Eq. (12) as follow:

$$\left. \begin{aligned} W_g(\varphi_g) &\implies \lambda\,W_g(\varphi_g) = \lambda\left\{\mathfrak{s}\big[\,|\,\varphi_g\,|-0.5\,\big] + 2\,\mathfrak{s}\big[\,|\,\varphi_g\,|-10\,\big]\right\}, \\ W_h(\psi_h) &\implies (1-\lambda)\,W_h(\psi_h) = (1-\lambda)\left\{-0.05\,\mathfrak{s}\big[\,|\,\psi_h\,|-0.5\,\big] - 0.1\,\mathfrak{s}\big[\,|\,\psi_h\,|-10\,\big]\right\}. \end{aligned} \right\} \quad (15)$$

Boundary condition

In this paper, we apply the zero-flux (Neumann) boundary condition to the states $v_{i,j}$ and $x_{i,j}$ in the *double-layer* autonomous Van der Pol CNN equations (14):

$$\left. \begin{aligned} v_{i,0} &\triangleq v_{i,0} = v_{i,1}, & i &= 1, 2, \cdots, N \\ v_{i,N+1} &\triangleq v_{i,N+1} = v_{i,N}, & i &= 1, 2, \cdots, N \\ v_{0,j} &\triangleq v_{0,j} = v_{1,j}, & j &= 1, 2, \cdots, M \\ v_{N+1,j} &\triangleq v_{N+1,j} = v_{N,j}, & j &= 1, 2, \cdots, M \\ x_{i,0} &\triangleq x_{i,0} = x_{i,1}, & i &= 1, 2, \cdots, N \\ x_{i,N+1} &\triangleq x_{i,N+1} = x_{i,N}, & i &= 1, 2, \cdots, N \\ x_{0,j} &\triangleq x_{0,j} = x_{1,j}, & j &= 1, 2, \cdots, M \\ vx_{N+1,j} &\triangleq x_{N+1,j} = x_{N,j}, & j &= 1, 2, \cdots, M. \end{aligned} \right\} \quad (16)$$

Under the condition (16), there is no current flow from the boundary in the border cells, since the terminal current i_g and voltage v_g of the memristors are zero at the boundary. That is, the boundary does not affect the dynamics of the *double-layer* autonomous Van der Pol CNN equations (14) (see [1] for more details).

Computer simulations

In order to obtain the solutions of the *double-layer* autonomous Van der Pol CNN equations (14), we assume the followings:

- The initial condition $v_{i,j}(0)$ is given by a gray-scale random noise image in Fig. 3, where the luminance value of the pixel is coded as gray $\rightarrow (-1,\ 1)$.

- $x_{i,j}(0) = 0$, $\varphi_{i,j}(0) = 0$, and $\psi_{i,j}(0) = 0$.

- The boundary condition for the state $v_{i,j}$ is given by Eq. (16).

Furthermore, we use the simple *Euler method*[3] and the *synchronous parallel model*[4] to find the solutions of the *double-layer* autonomous Van der Pol CNN equations (14). Then, from our computer simulations, we obtain Figs. 4 and 5, which show the nonlinear waves for the state $v_{i,j}$ and $x_{i,j}$, respectively. Observe that the *double-layer* autonomous Van der Pol CNN equations (14) can exhibit the complex nonlinear waves and interesting bifurcation phenomena:

1. The nonlinear wave for $\lambda = 0$ is evolving continuously, and then a *new* nonlinear wave appears by increasing λ. It finally changes to the nonlinear wave for $\lambda = 1$.

2. The *double-layer* autonomous Van der Pol CNN equations (14) for $0 < \lambda < 1$ can exhibit different nonlinear waves from those for the *single-layer* autonomous CNN equations (defined by $\lambda = 1$ and $\lambda = 0$). In particular, the nonlinear waves for $\lambda = 0.6, 0.7, 0.8, 0.9, 0.922$ appear quite different from the nonlinear waves in the single-layer autonomous CNN.

3. The nonlinear waves for $\lambda = 0.99$ and 0.995 seem to be developed by the interaction with the two nonlinear waves caused by the first layer and the second layer.

4. The *double-layer* autonomous Van der Pol CNN (14) seems to exhibit the sensitive dependence on the homotopy parameter λ. Observe that in the neighborhood of $\lambda = 0.995$, a small change of λ can result in large differences in a later state.

Thus, the *double-layer* autonomous Van der Pol CNN equations (14) can exhibit interesting deformation behaviors of the nonlinear waves by the homotopy method, and we can control the complexity of the nonlinear waves by using the homotopy parameter λ.

We note that in order to view the dynamic patterns clearly, we coded the state $v_{i,j}$ as follows: the color evolves continuously through black, blue, green, and red, as $v_{i,j}$ increases. In some other examples, we also coded the wave patterns in *reverse order*, that is, red, green, blue, and black, since $v_{i,j}(t)$ is oscillating (that is, it is always changing). Furthermore, we used the *nonlinear color curve* to emphasize the wave patterns by increasing or decreasing the intensity of the individual color.
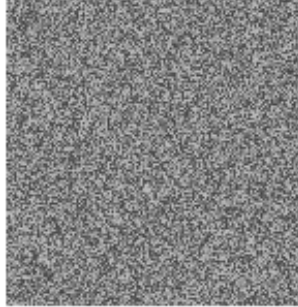

Figure 3: Image of the initial condition, which is a gray-scale random noise image. The luminance value of the pixel is coded as gray $\rightarrow (-1,\ 1)$.

---

[3]If the image size of the initial condition is $N \times M = 145 \times 150$, then we have to solve a system of $4 \times N \times M = 4 \times 145 \times 150 = 87000$ first-order differential equations. Thus, we used the simple Euler method for solving Eq. (14). The Euler method advances a solution through an interval h using derivative information. Thus, the *double-layer* autonomous Van der Pol CNN equations (14) are transformed into a discrete-time system (see [1] for more details).

[4]In the synchronous parallel model, the state of all the CNN cells is updated instantaneously at the beginning of each time step, and it is not changed until the next step. Only at the beginning of the next time step is the state of all CNN cells updated again. Since the Euler method can transform Eq. (14) into the discrete-time system, we can apply the synchronous parallel model to this discretized system.
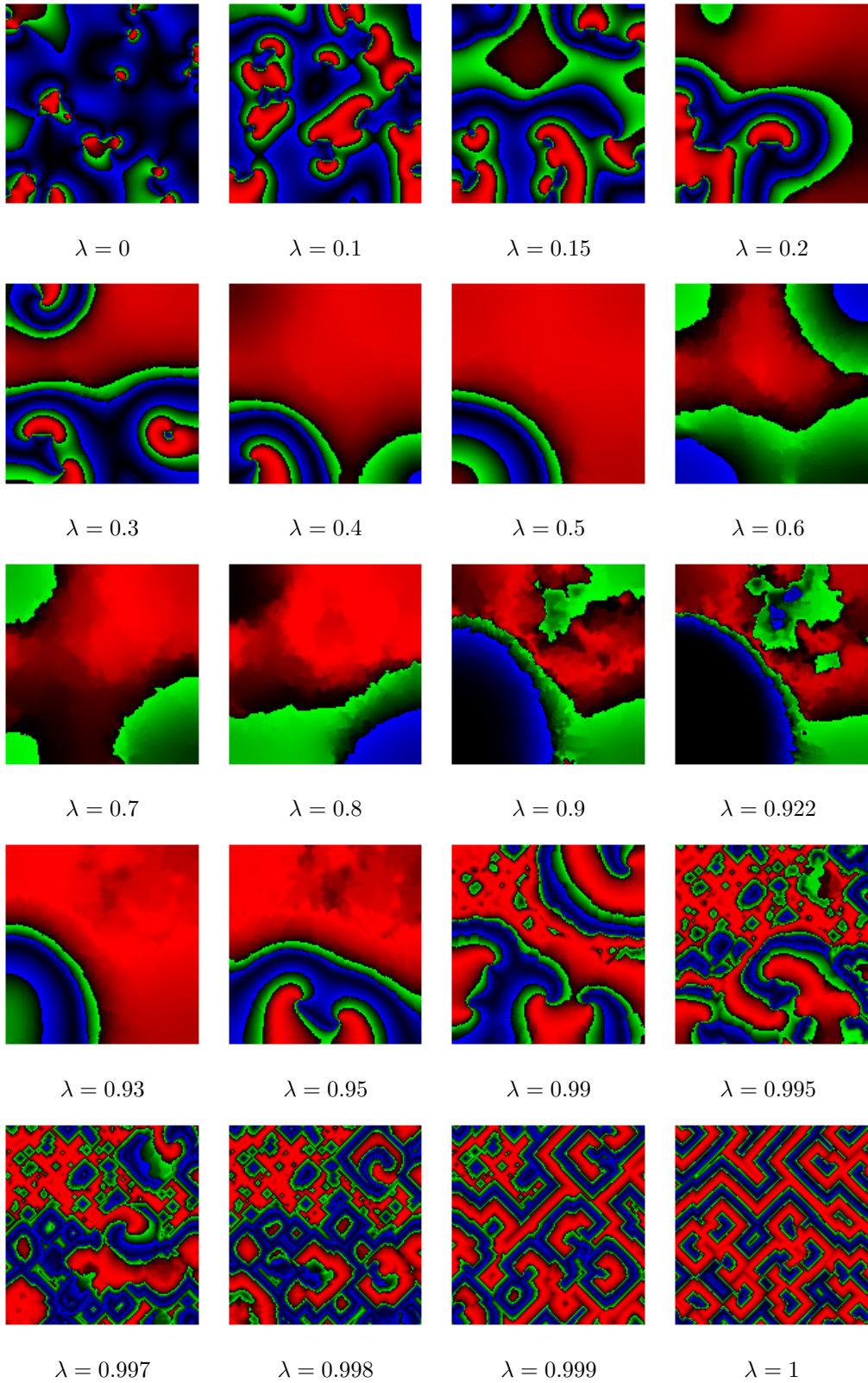
$\lambda = 0$ $\lambda = 0.1$ $\lambda = 0.15$ $\lambda = 0.2$

$\lambda = 0.3$ $\lambda = 0.4$ $\lambda = 0.5$ $\lambda = 0.6$

$\lambda = 0.7$ $\lambda = 0.8$ $\lambda = 0.9$ $\lambda = 0.922$

$\lambda = 0.93$ $\lambda = 0.95$ $\lambda = 0.99$ $\lambda = 0.995$

$\lambda = 0.997$ $\lambda = 0.998$ $\lambda = 0.999$ $\lambda = 1$

Figure 4: Nonlinear waves for the state $v_{i,j}$ in the *double-layer* autonomous Van der Pol CNN (14). Here, λ is the homotopy parameter. These figures are not static, but dynamic (always changing) images at the instant of $t = 4000$. The initial condition $v_{i,j}(0)$ is given by the random noise image in Fig. 3. The step size h of the Euler method is set to 0.02.
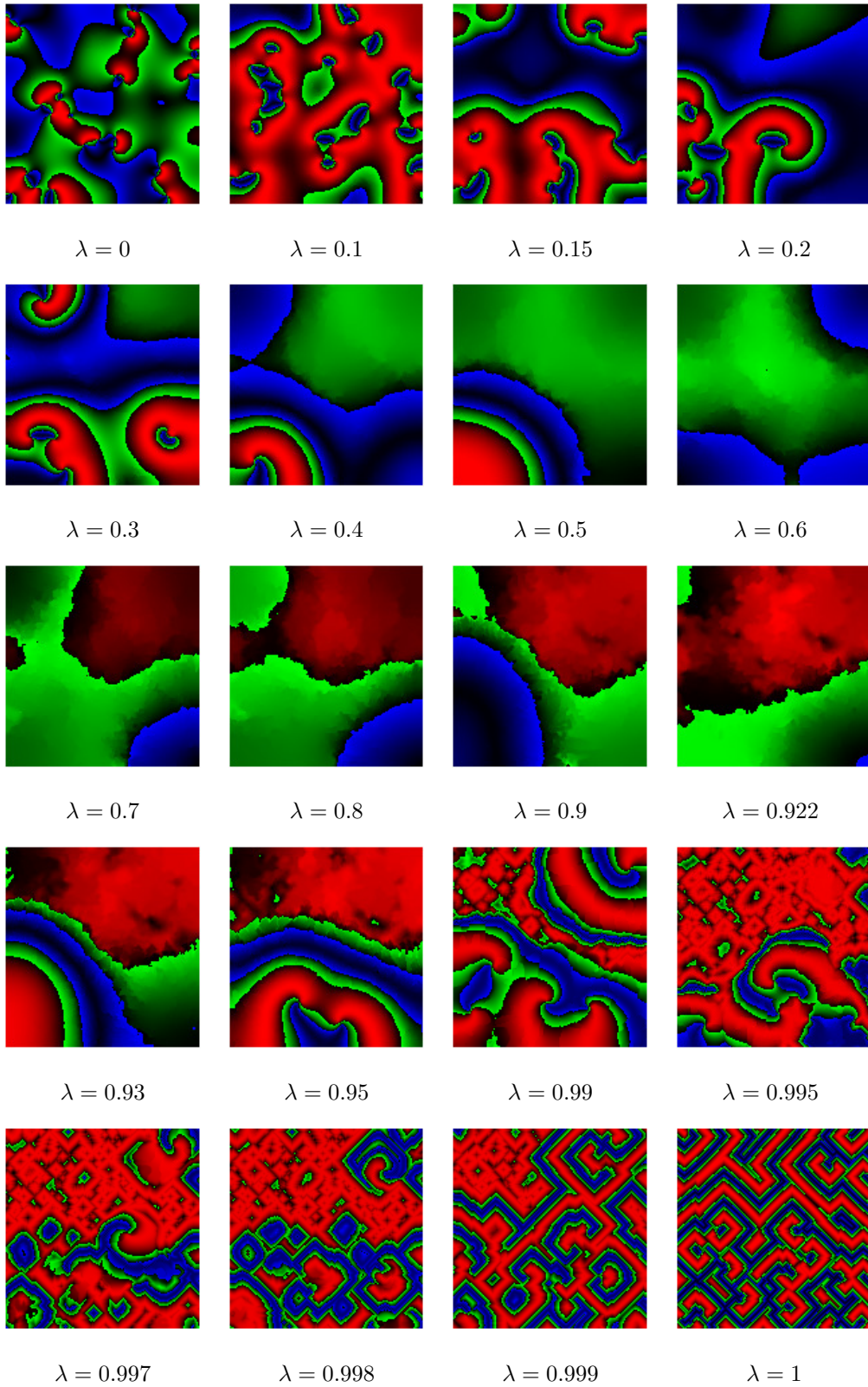
8

Figure 5: Nonlinear waves for the state $x_{i,j}$ in the *double-layer* autonomous Van der Pol CNN (14). Here, λ is the homotopy parameter. These figures are not static, but dynamic (always changing) images at the instant of $t = 4000$. The initial condition $v_{i,j}(0)$ is given by the random noise image in Fig. 3. The step size h of the Euler method is set to 0.02.
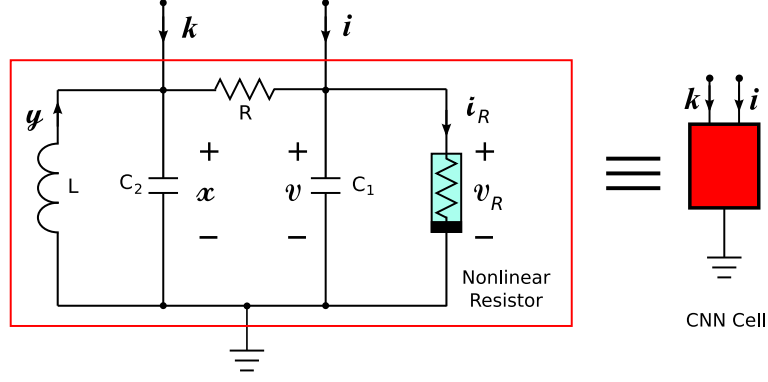
9

Figure 6: A dual synaptic-input CNN cell for Chua circuit. It contains five circuit elements: two linear capacitors C_1 and C_2, one linear inductor L, one linear resistor R, and one *nonlinear* resistor. The symbols i and k denote the synaptic input currents. The $v - i$ characteristic of the nonlinear resistor is given by $i_R = f(v_R) = \frac{1}{16} v_R{}^3 - \frac{7}{6} v_R$. The circuit parameters are given by $C_1 = \frac{1}{10}$, $C_2 = 1$, $L = \frac{1}{14}$, and $R = 1$.

2.2 Autonomous Chua circuit CNN

Consider the circuit in Fig. 6 (see [2], [3], and [4]). Its dynamics is given by

$$
\left.
\begin{aligned}
C_1 \frac{dv}{dt} &= \frac{x - v}{R} - f(v) + i, \\
C_2 \frac{dx}{dt} &= y - \frac{x - v}{R} + k, \\
L \frac{dy}{dt} &= -x,
\end{aligned}
\right\}
\tag{17}
$$

where v, x, and y denote the voltage across the capacitor C_1, the voltage across the capacitor C_2, and the current through the inductor L, respectively, and i and k denote the synaptic input currents. The parameters in Eq. (17) satisfy

$$
C_1 = \frac{1}{10}, \ C_2 = 1, \ L = \frac{1}{14}, \ R = 1,
\tag{18}
$$

and $v - i$ characteristic of the nonlinear resistor is given by

$$
i_R = f(v_R) = \frac{1}{16} v_R{}^3 - \frac{7}{6} v_R.
\tag{19}
$$

If we substitute Eqs. (18) and (19) into Eq. (17), then we obtain

$$
\left.
\begin{aligned}
\frac{dv}{dt} &= \alpha\big(x - v - f(v) + i\big), \\
\frac{dx}{dt} &= v - x + y + k, \\
\frac{dy}{dt} &= -\beta x,
\end{aligned}
\right\}
\tag{20}
$$

where $\alpha = 10$, $\beta = 14$, and $f(v)$ is a scalar function of a single variable v defined by

$$
f(v) = \frac{1}{16} v^3 - \frac{7}{6} v.
\tag{21}
$$

Assume next that the CNN cell is defined by Eq. (20). Then the dynamics of the *double-layer* autonomous CNN in Fig. 1 is described by

$$
\begin{aligned}
\frac{dv_{i,j}}{dt} &= \alpha\Big(x_{i,j} - v_{i,j} - f(v_{i,j}) + i_{i,j}\Big), \\[2mm]
\frac{dx_{i,j}}{dt} &= v_{i,j} - x_{i,j} + y_{i,j} + k_{i,j}, \\[2mm]
\frac{dy_{i,j}}{dt} &= -\beta x_{i,j}, \\[2mm]
\frac{d\varphi_{i,j}}{dt} &= v_{i,j}, \\[2mm]
\frac{d\psi_{i,j}}{dt} &= x_{i,j},
\end{aligned}
\tag{22}
$$

where $i = 1, 2, \cdots, N$, $j = 1, 2, \cdots, M$, the five state variables of the CNN cell $n_{i,j}$ are explained as follow:

- $v_{i,j}$ is the voltage across the capacitor C_1 in the CNN cell.
- $x_{i,j}$ is the voltage across the capacitor C_2 in the CNN cell.
- $y_{i,j}$ is the current though inductor in the CNN cell.
- $i_{i,j}$ is the current through the CNN cell from the first layer.
- $k_{i,j}$ is the current through the CNN cell from the second layer.

The current $i_{i,j}$ and $i_{k,j}$ is given by

$$
\begin{aligned}
i_{i,j} &= W_g(\varphi_{i-1,j} - \varphi_{i,j})(v_{i-1,j} - v_{i,j}) - W_g(\varphi_{i,j} - \varphi_{i+1,j})(v_{i,j} - v_{i+1,j}) \\[2mm]
&\quad + W_g(\varphi_{i,j-1} - \varphi_{i,j})(v_{i,j-1} - v_{i,j}) - W_g(\varphi_{i,j} - \varphi_{i,j+1})(v_{i,j} - v_{i,j+1}), \\[2mm]
k_{i,j} &= W_h(\psi_{i-1,j} - \psi_{i,j})(x_{i-1,j} - x_{i,j}) - W_h(\psi_{i,j} - \psi_{i+1,j})(x_{i,j} - x_{i+1,j}) \\[2mm]
&\quad + W_h(\psi_{i,j-1} - \psi_{i,j})(x_{i,j-1} - x_{i,j}) - W_h(\psi_{i,j} - \psi_{i,j+1})(x_{i,j} - x_{i,j+1}),
\end{aligned}
\tag{23}
$$

where $W_g(\varphi_g)$ and $W_h(\psi_h)$ denote the small-signal memductances of the voltage-controlled *ideal* memristors consisting the first layer and the second layer, respectively.

The terminal current i_g and voltage v_g of the memristors in the *first* layer are described by

$$
i_g = W_g(\varphi_g)\, v_g,
\tag{24}
$$

where φ_g is the flux of the memristor in the *first* layer, which satisfies $\dfrac{d\varphi_g}{dt} = v_g$ and $\varphi_g(0) = 0$. Assume that $W_g(\varphi_g)$ is given by

$$
\begin{aligned}
W_g(\varphi_g) &= -\mathfrak{s}\Big[\,|\varphi_g| - 0.5\Big] + 4\,\mathfrak{s}\Big[\,|\varphi_g| - 7\Big] \\[3mm]
&= \begin{cases}
0 & \text{for} \quad |\varphi_g| < 0.5, \\[3mm]
-1 & \text{for} \quad 0.5 \le |\varphi_g| < 7, \\[3mm]
3 & \text{for} \quad |\varphi_g| \ge 7.
\end{cases}
\end{aligned}
\tag{25}
$$

Then the memristors in the *first* layer are *locally active*, since the instantaneous power $p(t)$ satisfies

$$
p(t) = i_g(t)\, v_g(t) = W_g(\varphi_g(t))\, v_g(t)^2 = -v_g(t)^2 < 0,
\tag{26}
$$

for $0.5 < |\varphi_g| < 7$.

Similarly, the terminal current i_h and voltage v_h of the memristors in the *second* layer are described by

$$i_h = W_h(\psi_h)\, v_h, \tag{27}$$

where ψ_h is the flux of the memristor in the *second* layer, which satisfies $\dfrac{d\psi_h}{dt} = v_h$ and $\psi_h(0) = 0$. Assume that $W_h(\psi_h)$ is given by

$$W_h(\psi_h) \triangleq 0.2\, W_g(\psi_h) = -0.2\, \mathfrak{s}\big[\,|\psi_h| - 0.5\big] + 0.8\, \mathfrak{s}\big[\,|\psi_h| - 7\big]$$

$$= \begin{cases} \quad 0 & \text{for} \quad |\psi_h| < 0.5, \\[2mm] -0.2 & \text{for} \quad 0.5 \le |\psi_h| < 7, \\[2mm] \quad 0.6 & \text{for} \quad |\psi_h| \ge 7. \end{cases} \tag{28}$$

Then the memristors in the *second* layer are also *locally active*, since the instantaneous power $p(t)$ satisfies

$$p(t) = i_h(t)\, v_h(t) = W_g(\psi_h(t))\, v_h(t)^2 = -v_h(t)^2 < 0, \tag{29}$$

for $0.5 < |\psi_h| < 7$.

Boundary condition

We apply the zero-flux (Neumann) boundary condition to the states $v_{i,j}$ and $x_{i,j}$ in the *double-layer* autonomous Chua circuit CNN equations (22):

$$\left.\begin{aligned} v_{i,0} &\triangleq v_{i,0} = v_{i,1}, & i &= 1,2,\cdots,N \\[2mm] v_{i,N+1} &\triangleq v_{i,N+1} = v_{i,N}, & i &= 1,2,\cdots,N \\[2mm] v_{0,j} &\triangleq v_{0,j} = v_{1,j}, & j &= 1,2,\cdots,M \\[2mm] v_{N+1,j} &\triangleq v_{N+1,j} = v_{N,j}, & j &= 1,2,\cdots,M \end{aligned}\right\}$$

$$\left.\begin{aligned} x_{i,0} &\triangleq x_{i,0} = x_{i,1}, & i &= 1,2,\cdots,N \\[2mm] x_{i,N+1} &\triangleq x_{i,N+1} = x_{i,N}, & i &= 1,2,\cdots,N \\[2mm] x_{0,j} &\triangleq x_{0,j} = x_{1,j}, & j &= 1,2,\cdots,M \\[2mm] vx_{N+1,j} &\triangleq x_{N+1,j} = x_{N,j}, & j &= 1,2,\cdots,M. \end{aligned}\right\} \tag{30}$$

Under the condition (30), the boundary does not affect the dynamics of the autonomous *double-layer* Chua circuit CNN equations (22).

Computer simulations

In order to observe the bifurcation phenomena of the nonlinear waves, consider the following autonomous *double-layer* Chua circuit CNN equations:

$$\left.\begin{aligned}
\frac{dv_{i,j}}{dt} &= \alpha\Big(x_{i,j} - v_{i,j} - f(v_{i,j}) + \lambda\, i_{i,j}\Big), \\
\frac{dx_{i,j}}{dt} &= v_{i,j} - x_{i,j} + y_{i,j} + (1-\lambda)\, k_{i,j}, \\
\frac{dy_{i,j}}{dt} &= -\beta x_{i,j}, \\
\frac{d\varphi_{i,j}}{dt} &= v_{i,j}, \\
\frac{d\psi_{i,j}}{dt} &= x_{i,j},
\end{aligned}\right\} \tag{31}$$

where λ $(0 \le \lambda \le 1)$ is the homotopy parameter. Equation (31) can continuously deform the *second-layer* autonomous Chua circuit CNN equations into the *first-layer* autonomous Chua circuitCNN equations. In this case, we have to modify the memductances $W_g(\varphi_g)$ in Eq. (25) and $W_h(\psi_h)$ in Eq. (28) as follow:

$$\left.\begin{aligned}
W_g(\varphi_g) &\implies \lambda W_g(\varphi_g), \\
W_h(\psi_h) &\implies (1-\lambda)W_h(\psi_h).
\end{aligned}\right\} \tag{32}$$

In order to obtain the solutions of Eq. (31), we assume the followings:

- The initial conditions $v_{i,j}^*(0)$, $x_{i,j}^*(0)$, and $y_{i,j}^*(0)$ are equal to a gray-scale random noise image in Fig. 3. Here, $v_{i,j}(0) = 1.1\, v_{i,j}^*(0)$, $x_{i,j}(0) = 1.1\, x_{i,j}^*(0)$, and $y_{i,j}(0) = 1.1\, y_{i,j}^*(0)$.[5]

- $\varphi_{i,j}(0) = \psi_{i,j}(0) = 0$.

- The boundary conditions for the state $v_{i,j}$ and $x_{i,j}$ are given by Eq. (30).

Furthermore, we use the simple Euler method and the synchronous parallel model for solving Eq. (31). From our computer simulations, we obtain Figs. 7 and 8, which show the nonlinear waves for the state $v_{i,j}$ and $x_{i,j}$, respectively. Observe that the *double-layer* autonomous Chua circuit CNN equations (31) can exhibit the complex nonlinear waves:

1. Equation (31) $(0 < \lambda < 1)$ can exhibit different nonlinear waves from those for the *single-layer* autonomous Chua circuit CNN equations, which correspond to $\lambda = 1$ and $\lambda = 0$.

2. The nonlinear waves for $\lambda = 0.3$ in Figs. 7 and 8 appear quite different from the nonlinear waves in the single-layer autonomous CNN corresponding to $\lambda = 1$ and $\lambda = 0$. This seems to be resulted from the interaction with the two nonlinear waves caused by the first layer and the second layer.

Thus, the *double-layer* autonomous Chua circuit CNN equations (31) can exhibit interesting deformation behaviors of the nonlinear waves by the homotopy method, and we can control the complexity of the nonlinear waves by using the homotopy parameter λ.

---

[5]We used the *scaled* initial conditions in order to avoid an overflow in the numerical simulations.
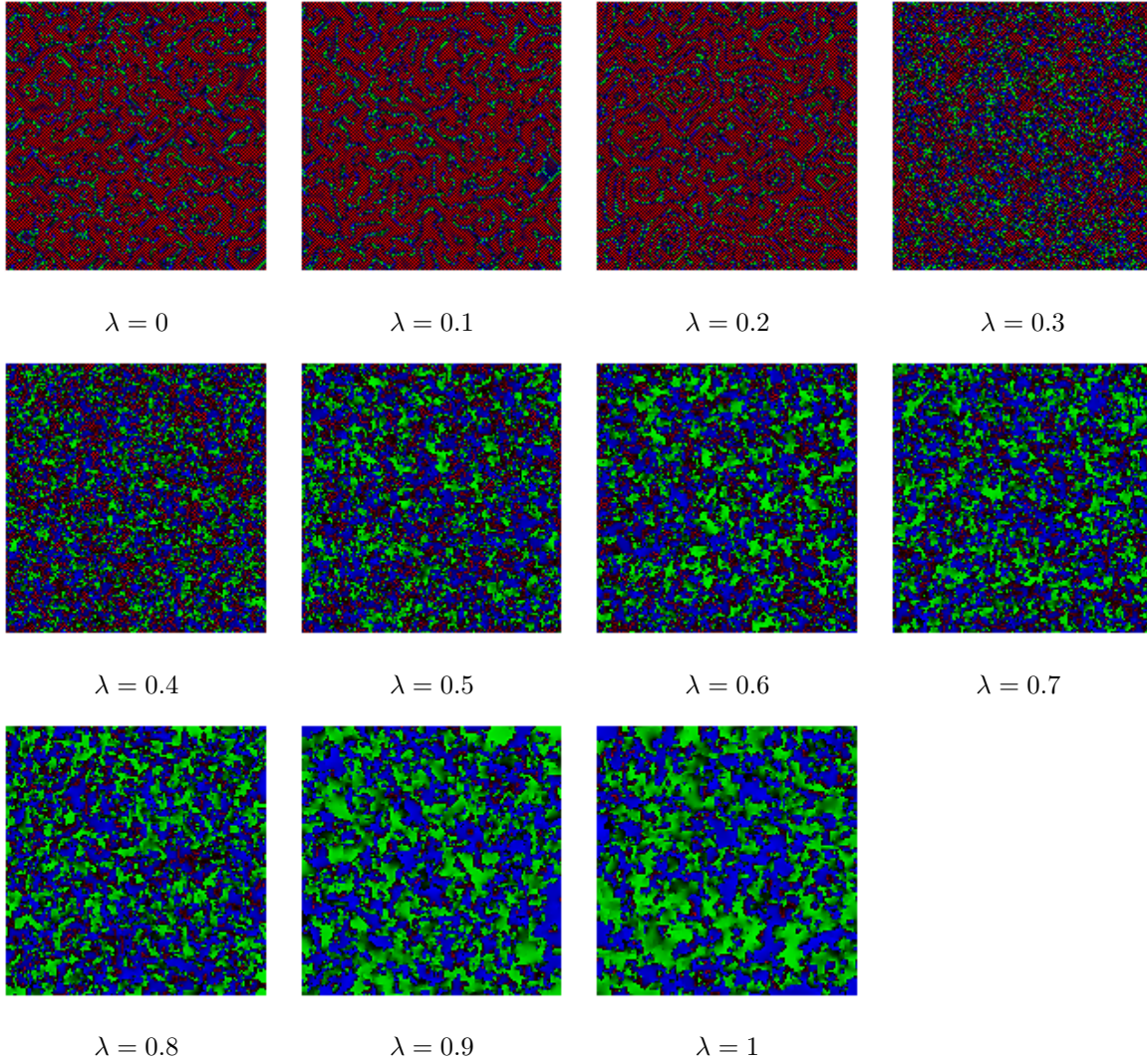
Figure 7: Nonlinear waves for the state $v_{i,j}$ in the *double-layer* autonomous Chua circuit CNN (31). Here, λ is the homotopy parameter. These figures are not static, but dynamic (always changing) images at the instant of $t = 1000$. The initial condition $v_{i,j}(0)$ is given by the random noise image in Fig. 3. The step size h of the Euler method is set to 0.005.
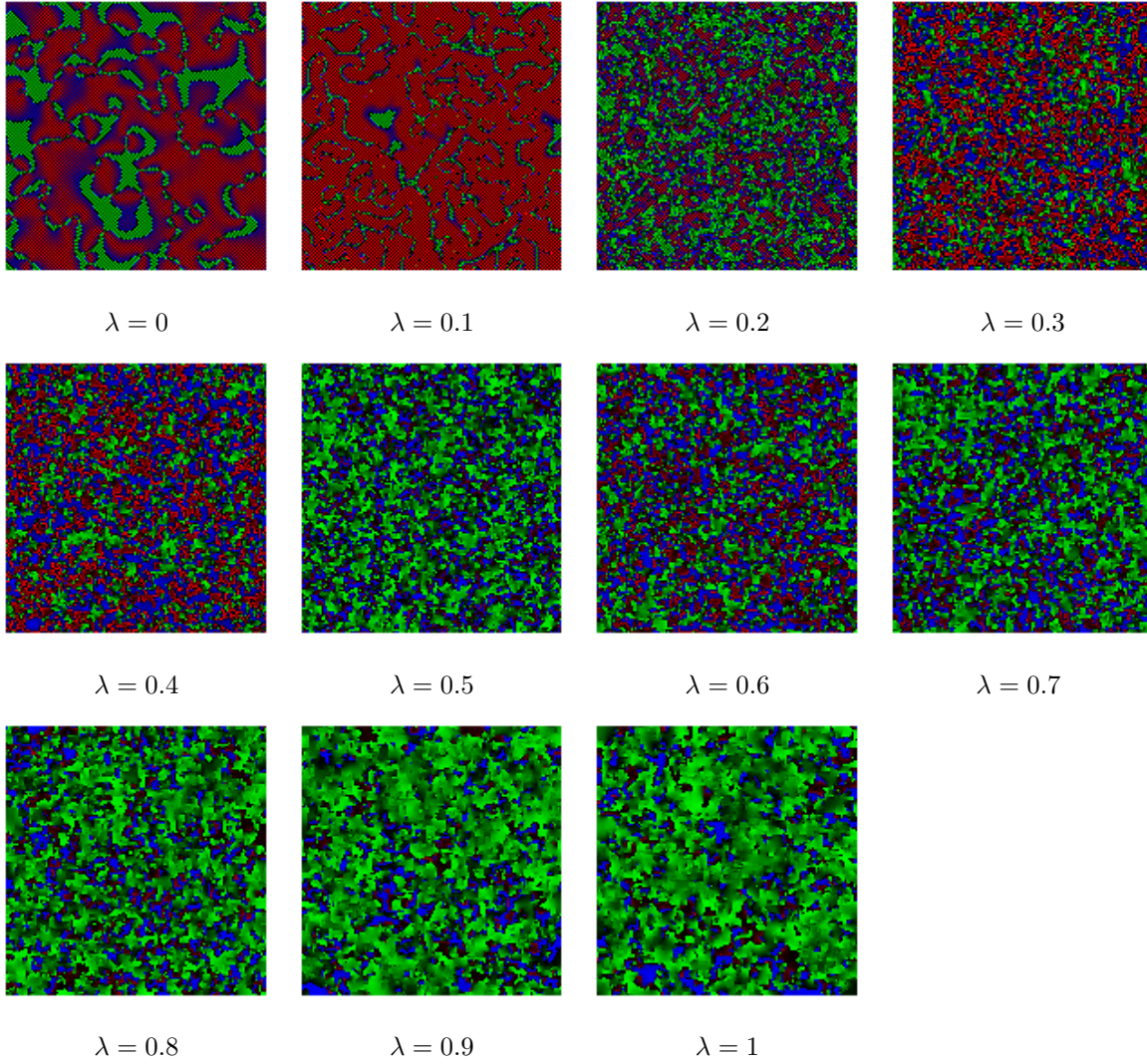
Figure 8: Nonlinear waves for the state $x_{i,j}$ in the *double-layer* autonomous Chua circuit CNN (31). Here, λ is the homotopy parameter. These figures are not static, but dynamic (always changing) images at the instant of $t = 1000$. The initial condition $v_{i,j}(0)$ is given by the random noise image in Fig. 3. The step size h of the Euler method is set to 0.005.

3 Two Layer Realization by a Single Synaptic-Input CNN Cell

Consider the three-element memristor circuit in Fig. 9 (see [1]). The dynamics of this circuit is given by

$$C\frac{dv}{dt} = -i_M + J + i, \tag{33}$$

where v denotes the voltage across the capacitor C, J denotes the direct current source, and i denotes the synaptic input current. Details of the terminal voltage v_M and the terminal current i_M of the voltage-controlled extended memristor [5] will be described in Sec. 3.1, where $v = v_M$.

We can realize the first layer by connecting three-element memristor circuit to the memristor grid as shown in Fig. 10. However, we cannot use this method to realize the second layer, since the three-element memristor circuit in Fig. 9 does not have the second synaptic-input. In this section, we realize it by using the CNN cell dynamics. That is, the extended memristors in the CNN cell are coupled to its four neighbors via the state equation, which can realize the dynamics of the second layer. We will show its details in Sec. 3.1.
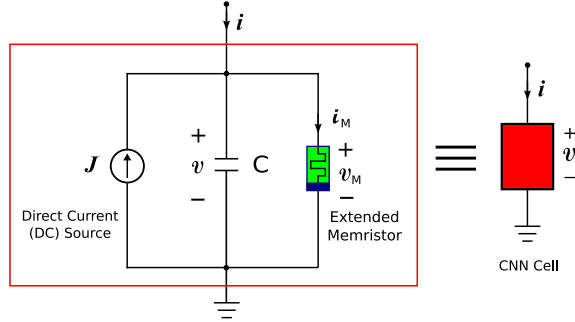

Figure 9: Three-element memristor circuit realization of a double synaptic-input CNN cell. It consists of a linear capacitor C, a direct current source J, a synaptic input current i, and a voltage-controlled extended memristor. Even though the CNN cell does not have the dual synaptic-inputs, the extended memristors in the CNN cell are coupled to its four neighbors via the state equation, which can realize the dynamics of the second layer.
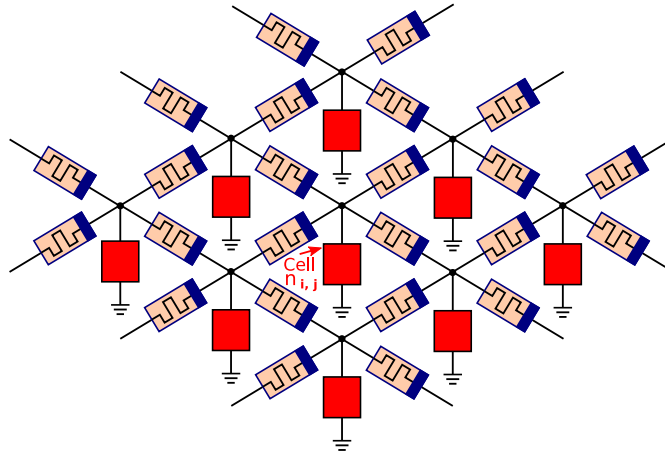

Figure 10: Autonomous CNN formed by connecting single synaptic-input CNN cells (colored in red) to each node of of the ideal memristor grid (colored in pink and navy). The second layer is realized by the dynamics of the extended memristor, which are coupled to its four neighbors via the state equation.

16

3.1 Autonomous Brusselator CNN

The dynamics of the autonomous Brusselator CNN having double layers can be formally described by (see [1, 2, 6])

$$
\left.
\begin{aligned}
\frac{dv_{i,j}}{dt} &= A + \{v_{i,j}x_{i,j} - (B+1)\}v_{i,j} + i_{i,j}, \\[2mm]
\frac{dx_{i,j}}{dt} &= B\,v_{i,j} - v_{i,j}{}^2\,x_{i,j} + k_{i,j}, \\[2mm]
\frac{dy_{i,j}}{dt} &= x_{i,j}, \\[2mm]
\frac{d\varphi_{i,j}}{dt} &= v_{i,j},
\end{aligned}
\right\}
\tag{34}
$$

where $A = 1$, $B = 3$, $i = 1, 2, \cdots, N$, $j = 1, 2, \cdots, M$, and the four state variables: $v_{i,j}$, $i_{i,j}$, $x_{i,j}$, and $\varphi_{i,j}$ of the CNN cell $n_{i,j}$ are explained as follow (see Figs. 9 and 10):

- $v_{i,j}$ is the voltage across the CNN cell, that is, the voltage across the capacitor C in the CNN cell.
- $i_{i,j}$ is the current through the CNN cell from the first layer.
- $k_{i,j}$ is the term corresponding to the *pseudo current* from the second layer.
- $x_{i,j}$ and $y_{i,j}$ are the state variables of the voltage-controlled *extended* memristor.
- $\varphi_{i,j}$ is the flux of the capacitor C in the CNN cell.

The current $i_{i,j}$ is given by

$$
\begin{aligned}
i_{i,j} =\ & W_g(\varphi_{i-1,j} - \varphi_{i,j})(v_{i-1,j} - v_{i,j}) - W_g(\varphi_{i,j} - \varphi_{i+1,j})(v_{i,j} - v_{i+1,j}) \\[2mm]
& + W_g(\varphi_{i,j-1} - \varphi_{i,j})(v_{i,j-1} - v_{i,j}) - W_g(\varphi_{i,j} - \varphi_{i,j+1})(v_{i,j} - v_{i,j+1}),
\end{aligned}
\tag{35}
$$

where $W_g(\varphi_g)$ denotes the small-signal memductances of the voltage-controlled *ideal* memristor consisting the *first* layer in Fig. 10. The terminal current i_g and voltage v_g of the memristors in the *first* layer are described by

$$
i_g = W_g(\varphi_g)\,v_g,
\tag{36}
$$

where φ_g is the flux of the memristor, which satisfies $\dfrac{d\varphi_g}{dt} = v_g$ and $\varphi_g(0) = 0$. We assume that $W_g(\varphi_g)$ is given by

$$
\begin{aligned}
W_g(\varphi_g) &= -0.25\,\mathfrak{s}\big[\,|\varphi_g| - 0.5\,\big] + 0.5\,\mathfrak{s}\big[\,|\varphi_g| - 10\,\big] \\[2mm]
&= \begin{cases}
0 & \text{for}\quad |\varphi_g| < 0.5, \\[2mm]
-0.25 & \text{for}\quad 0.5 \le |\varphi_g| < 10, \\[2mm]
0.25 & \text{for}\quad |\varphi_g| \ge 10.
\end{cases}
\end{aligned}
\tag{37}
$$

Then the memristors in the *first* layer are *locally active*, since the instantaneous power $p_g(t)$ satisfies

$$
p_g(t) = i_g(t)\,v_g(t) = W_g(\varphi_g(t))\,v_g(t)^2 < 0,
\tag{38}
$$

for $0.5 \le |\varphi_g| < 10$.

The term $k_{i,j}$ is defined by

$$
\begin{aligned}
k_{i,j} \quad = \quad & W_h(y_{i-1,j} - y_{i,j})(x_{i-1,j} - x_{i,j}) - W_h(y_{i,j} - y_{i+1,j})(x_{i,j} - x_{i+1,j}) \\
& + W_h(y_{i,j-1} - y_{i,j})(x_{i,j-1} - x_{i,j}) - W_h(y_{i,j} - y_{i,j+1})(x_{i,j} - x_{i,j+1}),
\end{aligned}
\tag{39}
$$

where $W_h(y)$ is a piecewise-linear function of y. We assume that $W_h(y)$ is given by

$$
W_h(y) \quad \overset{\triangle}{=} \quad 4\,W_g(y) = -0.1\,\mathfrak{s}\big[\,|\,y\,| - 0.5\,\big] + 0.2\,\mathfrak{s}\big[\,|\,y\,| - 10\,\big]
$$

$$
= \quad
\begin{cases}
0 & \text{for} \quad |y| < 0.5, \\[2mm]
-0.1 & \text{for} \quad 0.5 \leq |y| < 10, \\[2mm]
0.1 & \text{for} \quad |y| \geq 10,
\end{cases}
\tag{40}
$$

where y is the state variable of the memristor in the CNN cell, which satisfies $y(0) = 0$.

The *double-layer* autonomous Brusselator CNN (34) can be realized by the circuit in Figs. 9 and 10. The autonomous CNN in Fig. 10 is formed by connecting single synaptic-input CNN cells to each node of the ideal memristor grid. The second layer is realized by the dynamics of the extended memristor in Fig. 9, which are coupled to its four neighbors via the state equation. That is, the terminal voltage v_M and the terminal current i_M of the voltage-controlled *extended* memristor in Fig. 9 are described by (see [5, 6])

$$
\left.
\begin{aligned}
i_M \quad &= \quad -\big\{v_M\,x_{i,j} - (B+1)\big\}v_M, \\[2mm]
\frac{dx_{i,j}}{dt} \quad &= \quad B\,v_M - v_M{}^2\,x_{i,j} + k_{i,j}, \\[2mm]
\frac{dy_{i,j}}{dt} \quad &= \quad x_{i,j},
\end{aligned}
\right\}
\tag{41}
$$

where $v_M = v_{ij}$ and $k_{i,j}$ is considered to be the second layer term defined by Eq. (39), and it includes the states of four neighbors. The parameters of the three-element memristor circuit in Fig. 9 are given by $C = 1$ and $J = A = 1$, and we assumed that $B = 3$.

Boundary condition

We apply the zero-flux (Neumann) boundary condition to the state $v_{i,j}$ in the autonomous Brusselator CNN equations (34):

$$
\left.
\begin{aligned}
v_{i,0} \quad &\overset{\triangle}{=} \quad v_{i,0} = v_{i,1}, & i &= 1, 2, \cdots, N \\[2mm]
v_{i,N+1} \quad &\overset{\triangle}{=} \quad v_{i,N+1} = v_{i,N}, & i &= 1, 2, \cdots, N \\[2mm]
v_{0,j} \quad &\overset{\triangle}{=} \quad v_{0,j} = v_{1,j}, & j &= 1, 2, \cdots, M \\[2mm]
v_{N+1,j} \quad &\overset{\triangle}{=} \quad v_{N+1,j} = v_{N,j}, & j &= 1, 2, \cdots, M.
\end{aligned}
\right\}
\tag{42}
$$

We also assume that the state $x_{i,j}$ of the border cells satisfies the following relation:

$$\left.\begin{array}{rcll} x_{i,0} & \triangleq & x_{i,0} = x_{i,1}, & i = 1, 2, \cdots, N \\[2mm] x_{i,N+1} & \triangleq & x_{i,N+1} = x_{i,N}, & i = 1, 2, \cdots, N \\[2mm] x_{0,j} & \triangleq & x_{0,j} = x_{1,j}, & j = 1, 2, \cdots, M \\[2mm] vx_{N+1,j} & \triangleq & x_{N+1,j} = x_{N,j}, & j = 1, 2, \cdots, M. \end{array}\right\} \qquad (43)$$

Under these conditions, the boundary does not affect the dynamics of the *double-layer* autonomous Brusselator CNN equations (34).

Computer simulations

In order to observe the bifurcation phenomena of the nonlinear waves, consider the following *double-layer* autonomous Brusselator CNN equations:

$$\left.\begin{array}{rcl} \dfrac{dv_{i,j}}{dt} & = & A + \left\{ v_{i,j} x_{i,j} - (B+1) \right\} v_{i,j} + \lambda\, i_{i,j}, \\[3mm] \dfrac{dx_{i,j}}{dt} & = & B\, v_{i,j} - v_{i,j}{}^2\, x_{i,j} + (1-\lambda)\, k_{i,j}, \\[3mm] \dfrac{dy_{i,j}}{dt} & = & x_{i,j}, \\[3mm] \dfrac{d\varphi_{i,j}}{dt} & = & v_{i,j}, \end{array}\right\} \qquad (44)$$

where λ $(0 \le \lambda \le 1)$ is the homotopy parameter. Equation (44) can continuously deform the *second-layer* autonomous Brusselator CNN equations into the *first-layer* autonomous Brusselator CNN equations. In this case, we have to modify $W_g(\varphi_g)$ in Eq. (37) and $W_h(y$ in Eq. (28) as follow:

$$\left.\begin{array}{rcl} W_g(\varphi_g) & \Longrightarrow & \lambda W_g(\varphi_g), \\[3mm] W_h(y) & \Longrightarrow & (1-\lambda) W_h(y). \end{array}\right\} \qquad (45)$$

In order to obtain the solutions of the *double-layer* autonomous Brusselator CNN (44), we assume the followings:

- The initial condition $v_{i,j}(0)$ is given by a gray-scale random noise image in Fig. 3.

- $x_{i,j}(0) = y_{i,j}(0) = 0$ and $\varphi_{i,j}(0) = 0$.

- The boundary conditions for the states $v_{i,j}$ and $x_{i,j}$ are given by Eq. (42) and Eq. (43), respectively.

Furthermore, we use the simple Euler method and the synchronous parallel model for solving Eq. (44). From our computer simulations, we obtain Figs. 11 and 12, which show the nonlinear waves for the state $v_{i,j}$ and $x_{i,j}$, respectively. Observer that the *double-layer* autonomous Brusselator CNN (44) can exhibit the complex nonlinear waves and interesting bifurcation phenomena:

1. The *double-layer* autonomous Brusselator CNN equations $(0 < \lambda < 1)$ can exhibit different nonlinear waves from those for the *single-layer* autonomous Brusselator CNN equations, which correspond to $\lambda = 1$ and $\lambda = 0$.

2. The nonlinear waves for $\lambda = 0.6$, 0.7, 0.8 in Figs. 11 and 12 appear quite different from the nonlinear waves in the single-layer autonomous CNN. They are random noise like.

3. The nonlinear waves for $\lambda = 0.86$ in Figs. 11 and 12 seem to be developed, by the interaction with the two nonlinear waves caused by the first layer and the second layer.

4. The *double-layer* the autonomous Brusselator CNN (44) seems to exhibit the sensitive dependence on the homotopy parameter λ. Observe that in the neighborhood of $\lambda = 0.8$, a small change of λ can result in large differences in a later state.

Thus, the *double-layer* autonomous Brusselator CNN equations (44) can exhibit interesting deformation behaviors of the nonlinear waves by the homotopy method, and we can control the complexity of the nonlinear waves by using the homotopy parameter λ.
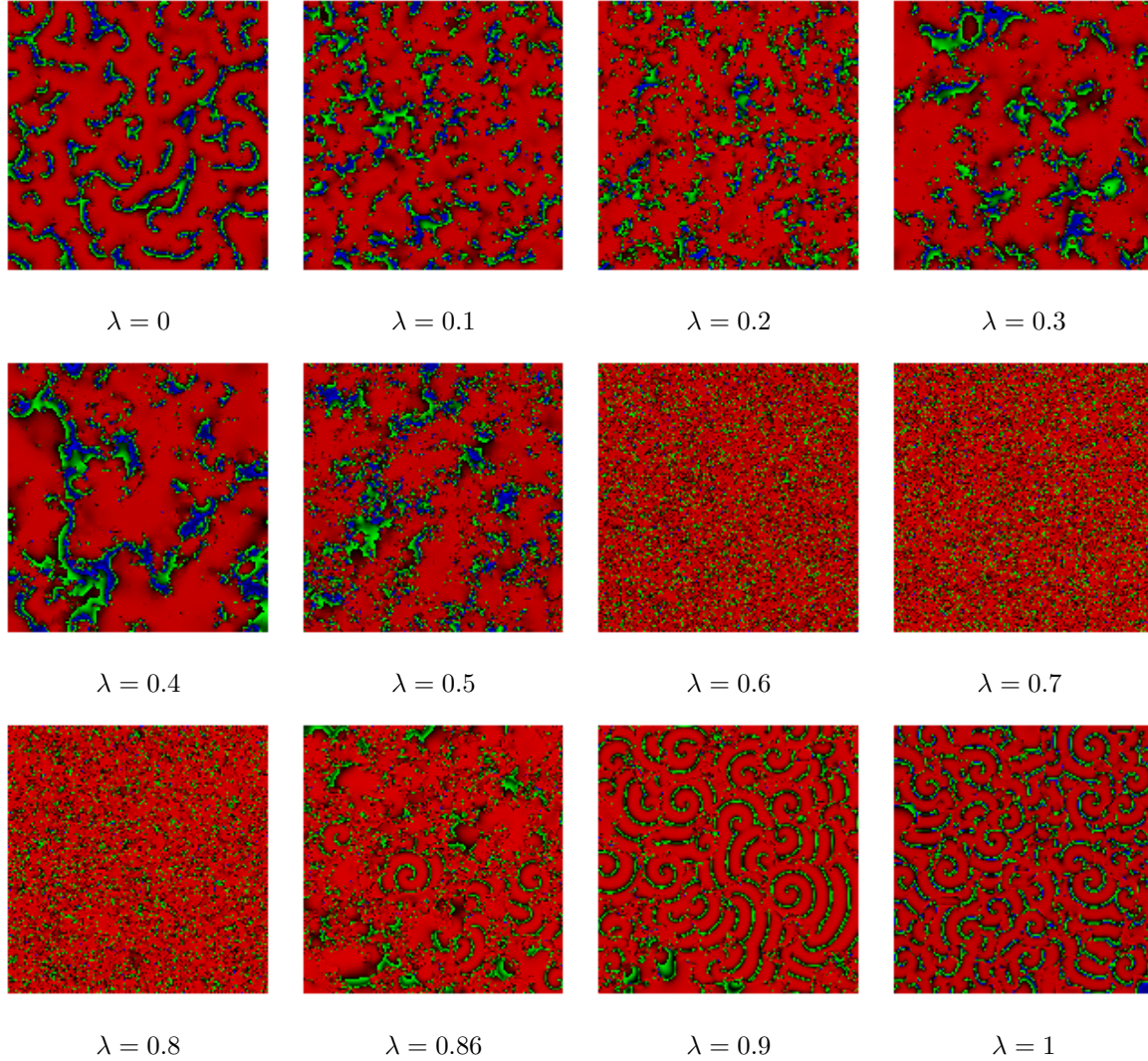

$\lambda = 0$	$\lambda = 0.1$	$\lambda = 0.2$	$\lambda = 0.3$
$\lambda = 0.4$	$\lambda = 0.5$	$\lambda = 0.6$	$\lambda = 0.7$
$\lambda = 0.8$	$\lambda = 0.86$	$\lambda = 0.9$	$\lambda = 1$

Figure 11: Nonlinear waves for the state $v_{i,j}$ in the *double-layer* autonomous Brusselator CNN (44). Here, λ is the homotopy parameter. These figures are not static, but dynamic (always changing) images at the instant of $t = 4000$. The initial condition $v_{i,j}(0)$ is given by the random noise image in Fig. 3. The step size h of the Euler method is set to 0.02.
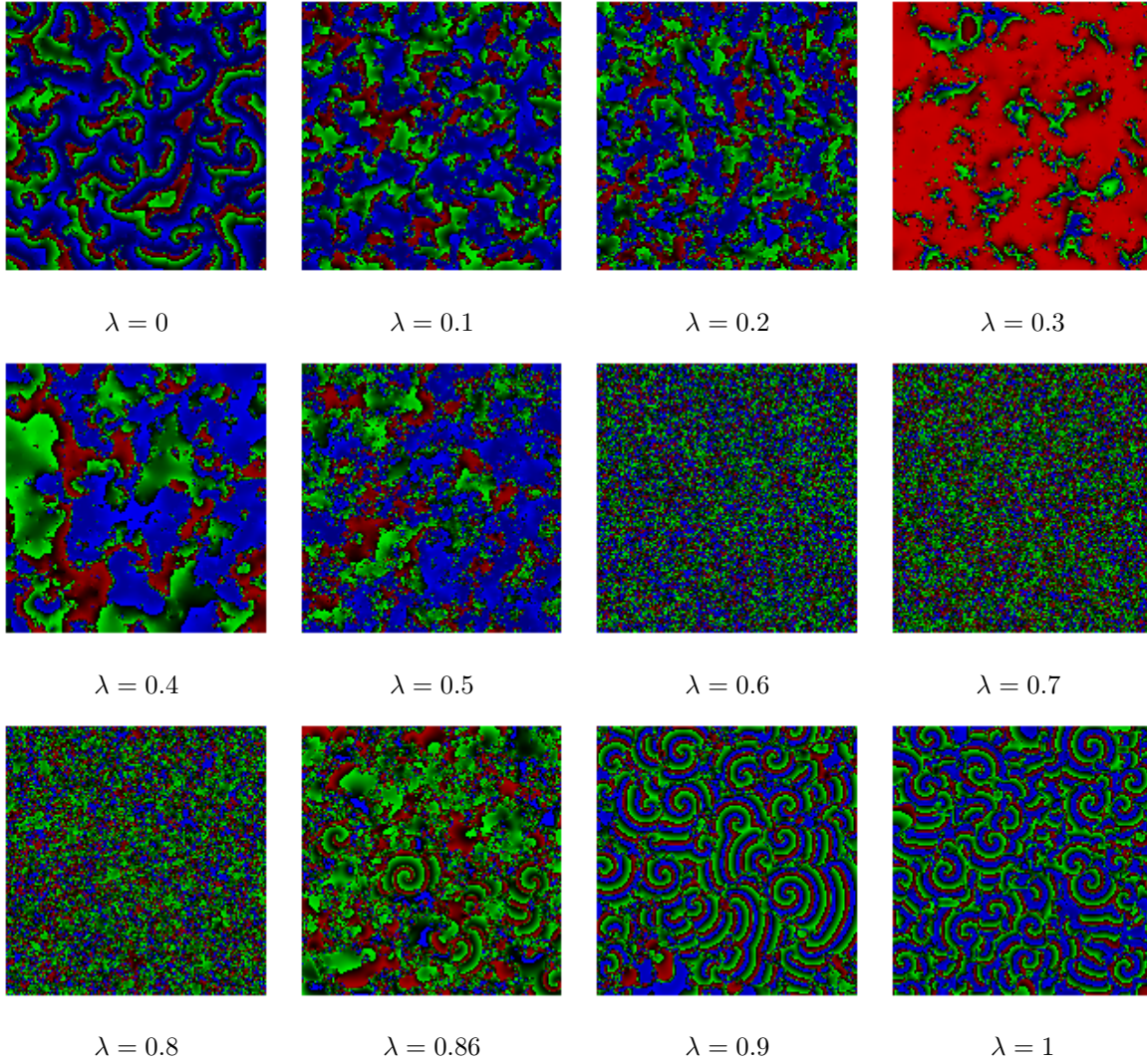
Figure 12: Nonlinear waves for the state $x_{i,j}$ in the *double-layer* autonomous Brusselator CNN (44). Here, λ is the homotopy parameter. These figures are not static, but dynamic (always changing) images at the instant of $t = 4000$. The initial condition $v_{i,j}(0)$ is given by the random noise image in Fig. 3. The step size h of the Euler method is set to 0.02.

3.2 Autonomous Rössler CNN

The dynamics of the autonomous Rössler CNN having double layers can be formally described by (see [1])

$$
\left.\begin{aligned}
\frac{dv_{i,j}}{dt} &= b + (x_{i,j} - c)\,v_{i,j} + i_{i,j}, \\
\frac{dx_{i,j}}{dt} &= y_{i,j} + a\,x_{i,j} + k_{i,j}, \\
\frac{dy_{i,j}}{dt} &= -x_{i,j} - v, \\
\frac{dz_{i,j}}{dt} &= y_{i,j}, \\
\frac{d\varphi_{i,j}}{dt} &= v_{i,j},
\end{aligned}\right\} \tag{46}
$$

where $a = 0.1$, $b = 0.1$, and $c = 14$, $i = 1, 2, \cdots, N$, $j = 1, 2, \cdots, M$, and the five state variables of the CNN cell $n_{i,j}$ are explained as follow (see Figs. 9 and 10):

- $v_{i,j}$ is the voltage across the CNN cell, that is, the voltage across the capacitor C in the CNN cell.
- $i_{i,j}$ is the current through the CNN cell from the first layer.
- $k_{i,j}$ is the term corresponding to the *pseudo current* from the second layer.
- $x_{i,j}$, $y_{i,j}$ and $z_{i,j}$ are the state variables of the voltage-controlled *extended* memristor in the CNN cell
- $\varphi_{i,j}$ is the flux of the capacitor C in the CNN cell.

The current $i_{i,j}$ in Eq. (46) is given by

$$
\begin{aligned}
i_{i,j} &= W_g(\varphi_{i-1,j} - \varphi_{i,j})(v_{i-1,j} - v_{i,j}) - W_g(\varphi_{i,j} - \varphi_{i+1,j})(v_{i,j} - v_{i+1,j}) \\
&\quad + W_g(\varphi_{i,j-1} - \varphi_{i,j})(v_{i,j-1} - v_{i,j}) - W_g(\varphi_{i,j} - \varphi_{i,j+1})(v_{i,j} - v_{i,j+1}),
\end{aligned} \tag{47}
$$

where $W_g(\varphi_g)$ denotes the small-signal memductance of the voltage-controlled *ideal* memristors consisting the grid. The terminal current i_g and voltage v_g of the above memristors are described by

$$
i_g = W_g(\varphi_g)\,v_g, \tag{48}
$$

where φ_g is the flux of the ideal memristor, which satisfies $\dfrac{d\varphi_g}{dt} = v_g$ and $\varphi_g(0) = 0$. We assume that $W_g(\varphi_g)$ is given by

$$
\begin{aligned}
W_g(\varphi_g) &= 2\mathfrak{s}\big[\,|\varphi_g| - 0.5\,\big] + \mathfrak{s}\big[\,|\varphi_g| - 1\,\big] \\[4pt]
&= \begin{cases}
0 & \text{for} \quad |\varphi_g| < 0.5, \\
2 & \text{for} \quad 0.5 \le |\varphi_g| < 10, \\
3 & \text{for} \quad |\varphi_g| \ge 10,
\end{cases}
\end{aligned} \tag{49}
$$

where φ_g is the flux of the memristor in the first layer, which satisfies $\dfrac{d\varphi_g}{dt} = v_g$ and $\varphi_g(0) = 0$. Then the memristors in the first layer are *passive*, since the instantaneous power $p_g(t)$ satisfies

$$
p_g(t) = i_g(t)\,v_g(t) = W_g(\varphi_g(t))\,v_g(t)^2 \ge 0. \tag{50}
$$

The term $k_{i,j}$ is defined by

$$
\begin{aligned}
k_{i,j} &= W_h(y_{i-1,j} - y_{i,j})(x_{i-1,j} - x_{i,j}) - W_h(y_{i,j} - y_{i+1,j})(x_{i,j} - x_{i+1,j}) \\
&\quad + W_h(y_{i,j-1} - y_{i,j})(x_{i,j-1} - x_{i,j}) - W_h(y_{i,j} - y_{i,j+1})(x_{i,j} - x_{i,j+1}),
\end{aligned} \tag{51}
$$

where $W_h(y)$ is a function of y. We assume that $W_h(y)$ is given by

$$W_h(y) \quad \triangleq \quad W_g(y) = 2\mathfrak{s}\big[\,|\,y\,| - 0.5\,\big] + \mathfrak{s}\big[\,|\,y\,| - 10\,\big]$$

$$= \begin{cases} 0 & \text{for} \quad |y| < 0.5, \\ 2 & \text{for} \quad 0.5 \le |y| < 10, \\ 3 & \text{for} \quad |y| \ge 10, \end{cases} \tag{52}$$

where y is the state variable of the memristor in the CNN cell, which satisfies $y(0) = 0$.

The *double-layer* autonomous Rössler CNN (46) can be realized by the circuit in Figs. 9 and 10. The second layer is realized by the dynamics of the extended memristor, which are coupled to its four neighbors via the state equation. That is, the terminal voltage v_M and the terminal current i_M of the voltage-controlled *extended* memristor in Fig. 9 are described by

$$\left. \begin{aligned} i_M &= -(x_{i,j} - c)\,v_M, \\ \frac{dx_{i,j}}{dt} &= y_{i,j} + a\,x_{i,j} + k_{i,j}, \\ \frac{dy_{i,j}}{dt} &= -x_{i,j} - v, \\ \frac{dz_{i,j}}{dt} &= y_{i,j}, \end{aligned} \right\} \tag{53}$$

where $v_M = v_{ij}$ and $k_{i,j}$ is considered to be the second layer term, which is defined by Eq. (51). The parameters in Fig. 9 are given by $C = 1$ and $J = b = 0.1$, and we assumed that $a = 0.1$ and $c = 14$,

Boundary condition

We apply the zero-flux (Neumann) boundary condition to the state $v_{i,j}$ in the *double-layer* autonomous Rössler CNN equations (46):

$$\left. \begin{aligned} v_{i,0} &\triangleq v_{i,0} = v_{i,1}, & i = 1, 2, \cdots, N \\ v_{i,N+1} &\triangleq v_{i,N+1} = v_{i,N}, & i = 1, 2, \cdots, N \\ v_{0,j} &\triangleq v_{0,j} = v_{1,j}, & j = 1, 2, \cdots, M \\ v_{N+1,j} &\triangleq v_{N+1,j} = v_{N,j}, & j = 1, 2, \cdots, M. \end{aligned} \right\} \tag{54}$$

We assume that the state $x_{i,j}$ of the border cells satisfies the following relation:

$$\left. \begin{aligned} x_{i,0} &\triangleq x_{i,0} = x_{i,1}, & i = 1, 2, \cdots, N \\ x_{i,N+1} &\triangleq x_{i,N+1} = x_{i,N}, & i = 1, 2, \cdots, N \\ x_{0,j} &\triangleq x_{0,j} = x_{1,j}, & j = 1, 2, \cdots, M \\ vx_{N+1,j} &\triangleq x_{N+1,j} = x_{N,j}, & j = 1, 2, \cdots, M. \end{aligned} \right\} \tag{55}$$

Under these conditions, the boundary does not affect the dynamics of the *double-layer* autonomous Rössler CNN equations.

Computer simulations

In order to observe the bifurcation phenomena of the nonlinear waves, consider the following autonomous Rössler CNN equations:

$$\left.\begin{aligned}
\frac{dv_{i,j}}{dt} &= A + \{v_{i,j}x_{i,j} - (B+1)\}v_{i,j} + \lambda\, i_{i,j}, \\
\frac{dx_{i,j}}{dt} &= B\, v_{i,j} - v_{i,j}{}^2\, x_{i,j} + (1-\lambda)\, k_{i,j}, \\
\frac{dy_{i,j}}{dt} &= x_{i,j}, \\
\frac{d\varphi_{i,j}}{dt} &= v_{i,j},
\end{aligned}\right\} \tag{56}$$

where λ $(0 \leq \lambda \leq 1)$ is the homotopy parameter. Equation (56) can continuously deform the *second-layer* autonomous Rössler CNN equations into the *first-layer* autonomous CNN equations. In this case, we have to modify $W_g(\varphi_g)$ in Eq. (49) and $W_h(y)$ in Eq. (52) as follow:

$$\left.\begin{aligned}
W_g(\varphi_g) &\implies \lambda W_g(\varphi_g), \\
W_h(y) &\implies (1-\lambda)W_h(y).
\end{aligned}\right\} \tag{57}$$

In order to obtain the solutions of the *double-layer* autonomous Rössler CNN (56), we assume the followings:

- The initial conditions $v_{i,j}^*(0)$ and $x_{i,j}^*(0)$ are equal to a gray-scale random noise image in Fig. 3. Here, $v_{i,j}(0) = 1.1\, v_{i,j}^*(0)$ and $x_{i,j}(0) = 1.1\, x_{i,j}^*(0)$.[6]

- $\varphi_{i,j}(0) = y_{i,j}(0) = 0$.

- The boundary conditions for the state $v_{i,j}$ and $x_{i,j}$ are given by Eqs. (54) and (55), respectively.

Furthermore, we use the simple Euler method and the synchronous parallel model for solving Eq. (56). From our computer simulations, we obtain Figs. 13 and 14, which show the nonlinear waves for the state $v_{i,j}$ and $x_{i,j}$, respectively. Observer that the *double-layer* autonomous Rössler CNN equations (56) can exhibit the complex nonlinear waves and interesting bifurcation phenomena:

1. The *double-layer* autonomous Rössler CNN equations (56) $(0 < \lambda < 1)$ can exhibit different nonlinear waves from those for the *single-layer* autonomous Rössler CNN equations, which correspond to $\lambda = 1$ and $\lambda = 0$.

2. The nonlinear waves for $\lambda = 0.78, 0.79, 0.8$ in Fig. 13 and those for $\lambda = 0.5, 0.6, 0.7, 0.8, 0.9$ in Fig. 14 appear quite different from the nonlinear waves in the single-layer autonomous CNN.

3. The nonlinear waves for $\lambda = 0.99$ in Fig. 13 and those for $\lambda = 0.997, 0.998$ in Fig. 14 seem to be developed, by the interaction with the two nonlinear waves caused by the first layer and the second layer.

4. The *double-layer* autonomous Rössler CNN equations (56) seems to exhibit the sensitive dependence on the homotopy parameter λ. Observe that in the neighborhood of $\lambda = 0.95$, a small change of λ can result in large differences in a later state.

Thus, the *double-layer* autonomous Rössler CNN equations (56) can exhibit interesting deformation behaviors of the nonlinear waves by the homotopy method, and we can control the complexity of the nonlinear waves by using the homotopy parameter λ.

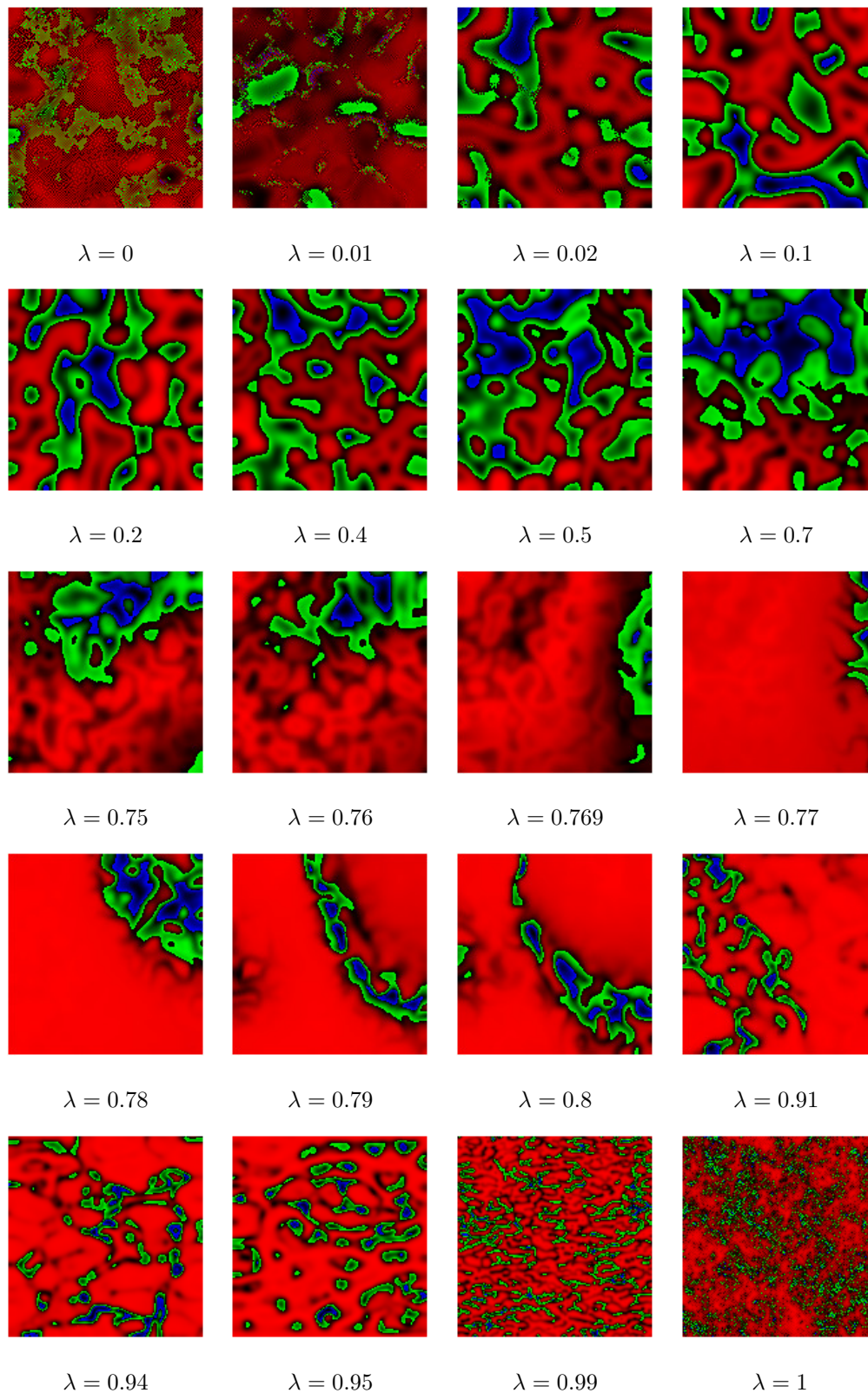[6]We used the scaled initial conditions in order to avoid an overflow in the numerical simulations.

Figure 13: Nonlinear waves for the state $v_{i,j}$ in the *double-layer* autonomous Rössler CNN (56). Here, λ is the homotopy parameter. These figures are not static, but dynamic (always changing) images at the instant of $t = 2000$. The initial condition $v_{i,j}(0)$ is given by the random noise image in Fig. 3. The step size h of the Euler method is set to 0.02.
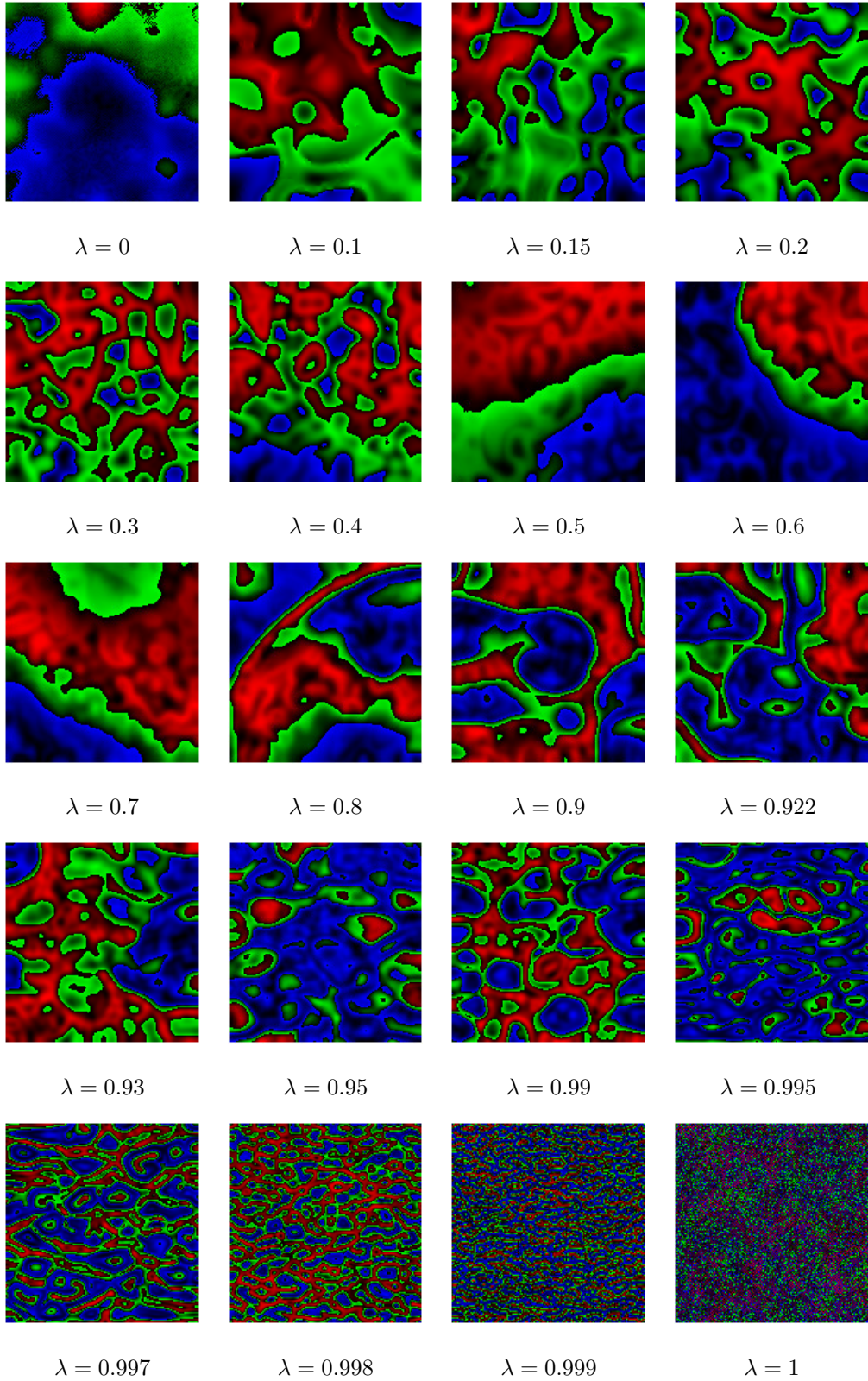
Figure 14: Nonlinear waves for the state $x_{i,j}$ in the *double-layer* autonomous Rössler CNN (56). Here, λ is the homotopy parameter. These figures are not static, but dynamic (always changing) images at the instant of $t = 2000$. The initial condition $v_{i,j}(0)$ is given by the random noise image in Fig. 3. The step size h of the Euler method is set to 0.02.

3.3 Autonomous Lotka-Volterra CNN

The dynamics of the autonomous Lotka-Volterra CNN having double layers can be formally described by (see [1])

$$
\left.
\begin{aligned}
\frac{dv_{i,j}}{dt} &= -(c\,x_{i,j} - d)\,v_{i,j} + i_{i,j}, \\
\frac{dx_{i,j}}{dt} &= (a - b\,v_{i,j} + v_{i,j})\,x_{i,j} + k_{i,j}, \\
\frac{d\varphi_{i,j}}{dt} &= v_{i,j},
\end{aligned}
\right\}
\tag{58}
$$

where $a = \dfrac{2}{3}$, $b = \dfrac{4}{3}$, and $c = d = 1$, $i = 1, 2, \cdots, N$, $j = 1, 2, \cdots, M$, and the four state variables of the CNN cell $n_{i,j}$ are explained as follow (see Figs. 9 and 10):

- $v_{i,j}$ is the voltage across the CNN cell, that is, the voltage across the capacitor C in the CNN cell.
- $i_{i,j}$ is the current through the CNN cell from the first layer.
- $k_{i,j}$ is the term corresponding to the *pseudo current* from the second layer.
- $x_{i,j}$ is the state variable of the voltage-controlled *extended* memristor.
- $\varphi_{i,j}$ is the flux of the capacitor C.

The current $i_{i,j}$ in Eq. (58) is given by

$$
\begin{aligned}
i_{i,j} &= W_g(\varphi_{i-1,j} - \varphi_{i,j})(v_{i-1,j} - v_{i,j}) - W_g(\varphi_{i,j} - \varphi_{i+1,j})(v_{i,j} - v_{i+1,j}) \\
&\quad + W_g(\varphi_{i,j-1} - \varphi_{i,j})(v_{i,j-1} - v_{i,j}) - W_g(\varphi_{i,j} - \varphi_{i,j+1})(v_{i,j} - v_{i,j+1}),
\end{aligned}
\tag{59}
$$

where $W_g(\varphi_g)$ denotes the small-signal memductance of the voltage-controlled *ideal* memristors consisting the grid. The terminal current i_g and voltage v_g of the above memristors are given by

$$
i_g = W_g(\varphi_g)\,v_g,
\tag{60}
$$

where φ_g is the flux of the ideal memristor, which satisfies $\dfrac{d\varphi_g}{dt} = v_g$ and $\varphi_g(0) = 0$. Assume that $W_g(\varphi_g)$ is given by

$$
\begin{aligned}
W_g(\varphi_g) &= \mathfrak{s}\big[\,|\varphi_g| - 0.5\big] - \mathfrak{s}\big[\,|\varphi_g| - 3\big] \\[4pt]
&= \begin{cases}
0 & \text{for} \quad |\varphi_g| < 0.5, \\[6pt]
1 & \text{for} \quad 0.5 \le |\varphi_g| < 3, \\[6pt]
0 & \text{for} \quad |\varphi_g| \ge 3.
\end{cases}
\end{aligned}
\tag{61}
$$

Then the ideal memristors consisting the grid are *passive*, since $W_g(\varphi_g) \ge 0$ and the instantaneous power $p(t)$ satisfies

$$
p(t) = i_g(t)\,v_g(t) = W_g(\varphi_g(t))\,v_g(t)^2 \ge 0.
\tag{62}
$$

Note that when $|\varphi_g|$ is greater than 3 or less than 0.5, the memductance $W_g(\varphi_g)$ becomes *zero*, and the terminal current i_g does not flow into the memristor.

The term $k_{i,j}$ is defined by

$$
\begin{aligned}
k_{i,j} &= W_h(y_{i-1,j} - y_{i,j})(x_{i-1,j} - x_{i,j}) - W_h(y_{i,j} - y_{i+1,j})(x_{i,j} - x_{i+1,j}) \\
&\quad + W_h(y_{i,j-1} - y_{i,j})(x_{i,j-1} - x_{i,j}) - W_h(y_{i,j} - y_{i,j+1})(x_{i,j} - x_{i,j+1}),
\end{aligned}
\tag{63}
$$

where $W_h(y)$ is a function of y. We assume that $W_h(y)$ is given by

$$W_h(y) \quad \overset{\triangle}{=} \quad W_g(y) = \mathfrak{s}\big[\,|\,y\,| - 0.5\,\big] - \mathfrak{s}\big[\,|\,y\,| - 3\,\big]$$

$$= \quad \begin{cases} 0 & \text{for} \quad |y| < 0.5, \\[2mm] 1 & \text{for} \quad 0.5 \le |y| < 10, \\[2mm] 0 & \text{for} \quad |y| \ge 10, \end{cases} \tag{64}$$

where y is the state variable of the memristor in the CNN cell, which satisfies $y(0) = 0$.

The *double-layer* autonomous Lotka-Volterra CNN (58) can be realized by the circuit in Figs. 9 and 10. The second layer is realized by the dynamics of the extended memristor, which are coupled to its four neighbors via the state equation. That is, the terminal voltage v_M and the terminal current i_M of the voltage-controlled *extended* memristor in Fig. 9 are described by

$$\left. \begin{aligned} i_M &= (c\,x_{i,j} - d)\,v_M, \\[2mm] \frac{dx_{i,j}}{dt} &= (a - b\,v_{i,j} + v_{i,j})\,x_{i,j} + k_{i,j}, \\[2mm] \frac{dy_{i,j}}{dt} &= x_{i,j}, \end{aligned} \right\} \tag{65}$$

where $v_M = v_{ij}$ and $k_{i,j}$ is considered to be the second layer term, which is defined by Eq. (63). The paremeters in Fig. 9 are given by $C = 1$ and $J = 0$, and we assumed than $a = \dfrac{2}{3}$, $b = \dfrac{4}{3}$, and $c = d = 1$.

Boundary condition

We apply the zero-flux (Neumann) boundary condition to the state $v_{i,j}$ in the autonomous *double-layer* Lotka-Volterra CNN equations (58):

$$\left. \begin{aligned} v_{i,0} &\overset{\triangle}{=} v_{i,0} = v_{i,1}, & i = 1, 2, \cdots, N \\[2mm] v_{i,N+1} &\overset{\triangle}{=} v_{i,N+1} = v_{i,N}, & i = 1, 2, \cdots, N \\[2mm] v_{0,j} &\overset{\triangle}{=} v_{0,j} = v_{1,j}, & j = 1, 2, \cdots, M \\[2mm] v_{N+1,j} &\overset{\triangle}{=} v_{N+1,j} = v_{N,j}, & j = 1, 2, \cdots, M. \end{aligned} \right\} \tag{66}$$

We assume that the state $x_{i,j}$ of the border cells satisfies the following relation:

$$\left. \begin{aligned} x_{i,0} &\overset{\triangle}{=} x_{i,0} = x_{i,1}, & i = 1, 2, \cdots, N \\[2mm] x_{i,N+1} &\overset{\triangle}{=} x_{i,N+1} = x_{i,N}, & i = 1, 2, \cdots, N \\[2mm] x_{0,j} &\overset{\triangle}{=} x_{0,j} = x_{1,j}, & j = 1, 2, \cdots, M \\[2mm] vx_{N+1,j} &\overset{\triangle}{=} x_{N+1,j} = x_{N,j}, & j = 1, 2, \cdots, M. \end{aligned} \right\} \tag{67}$$

Under these conditions, the boundary does not affect the dynamics of the *double-layer* autonomous Lotka-Volterra CNN equations.

Computer simulations

In order to observe the bifurcation phenomena of the nonlinear waves, consider the following *double-layer* autonomous Lotka-Volterra CNN equations:

$$\left.\begin{aligned}
\frac{dv_{i,j}}{dt} &= -(c\,x_{i,j} - d)\,v_{i,j} + \lambda i_{i,j}, \\
\frac{dx_{i,j}}{dt} &= (a - b\,v_{i,j} + v_{i,j})\,x_{i,j} + (1 - \lambda)k_{i,j}, \\
\frac{d\varphi_{i,j}}{dt} &= v_{i,j},
\end{aligned}\right\} \tag{68}$$

where λ ($0 \leq \lambda \leq 1$) is the homotopy parameter. Equation (68) can continuously deform the *second-layer* autonomous Lotka-Volterra CNN equations into the *first-layer* autonomous Lotka-Volterra CNN equations. In this case, we have to modify $W_g(\varphi_g)$ in Eq. (61) and $W_h(y)$ in Eq. (64) as follow:

$$\left.\begin{aligned}
W_g(\varphi_g) &\implies \lambda W_g(\varphi_g), \\
W_h(y) &\implies (1 - \lambda)W_h(y).
\end{aligned}\right\} \tag{69}$$

In order to obtain the solutions of the autonomous Lotka-Volterra CNN equations (68), we assume the followings:

- The initial conditions $v_{i,j}^*(0)$ and $x_{i,j}^*(0)$ are equal to a gray-scale random noise image in Fig. 3. Here, $v_{i,j}^*(0) = v_{i,j}(0) - 1.1$ and $x_{i,j}^*(0) = x_{i,j}(0) - 1.1$.[7]

- $\varphi_{i,j}(0) = y_{i,j}(0) = 0$.

- The boundary conditions for the state $v_{i,j}$ and $x_{i,j}$ are given by Eqs. (66) and (67), respectively.

Furthermore, we use the simple Euler method and the synchronous parallel model for solving Eq. (68). From our computer simulations, we obtain Figs. 15 and 16, which show the nonlinear waves for the state $v_{i,j}$ and $x_{i,j}$, respectively. Observe that the *double-layer* autonomous Lotka-Volterra CNN equations (68) can exhibit the complex nonlinear waves and interesting bifurcation phenomena:

1. The *double-layer* autonomous Lotka-Volterra CNN equations (68) ($0 < \lambda < 1$) can exhibit different nonlinear waves from those for the *single-layer* Lotka-Volterra CNN equations , which correspond to $\lambda = 1$ and $\lambda = 0$.

2. We can observe small isolated patterns when the homotopy parameter λ satisfies $\lambda = 0.8$, 0.91, 0.94 in the case of Fig. 15 and $\lambda = 0.78$, 0.79, 0.8, 0.91 in the case of Fig. 16. This seems to be resulted from the interaction with the two nonlinear waves caused by the first layer and the second layer.

Thus, the *double-layer* autonomous Lotka-Volterra CNN equations (68) can exhibit interesting deformation behaviors of the nonlinear waves by the homotopy method, and we can control the complexity of the nonlinear waves by using the homotopy parameter λ.

---

[7]We shifted the initial conditions in order to avoid an overflow in the numerical simulations.
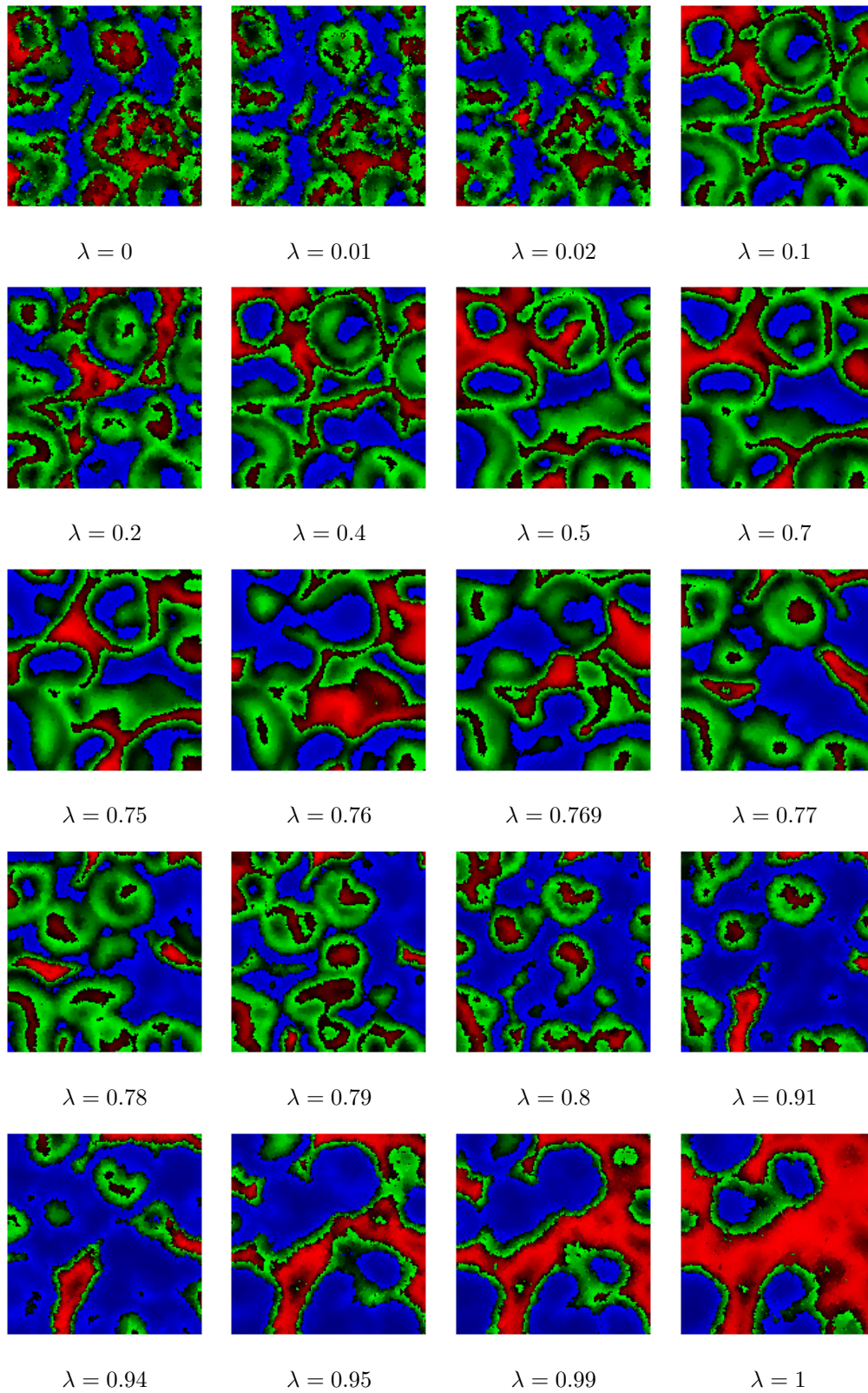
Figure 15: Nonlinear waves for the state $v_{i,j}$ in the *double-layer* autonomous Lotka-Volterra CNN (68). Here, λ is the homotopy parameter. These figures are not static, but dynamic (always changing) images at the instant of $t = 500$. The initial condition $v_{i,j}(0)$ is given by the random noise image in Fig. 3. The step size h of the Euler method is set to 0.002.
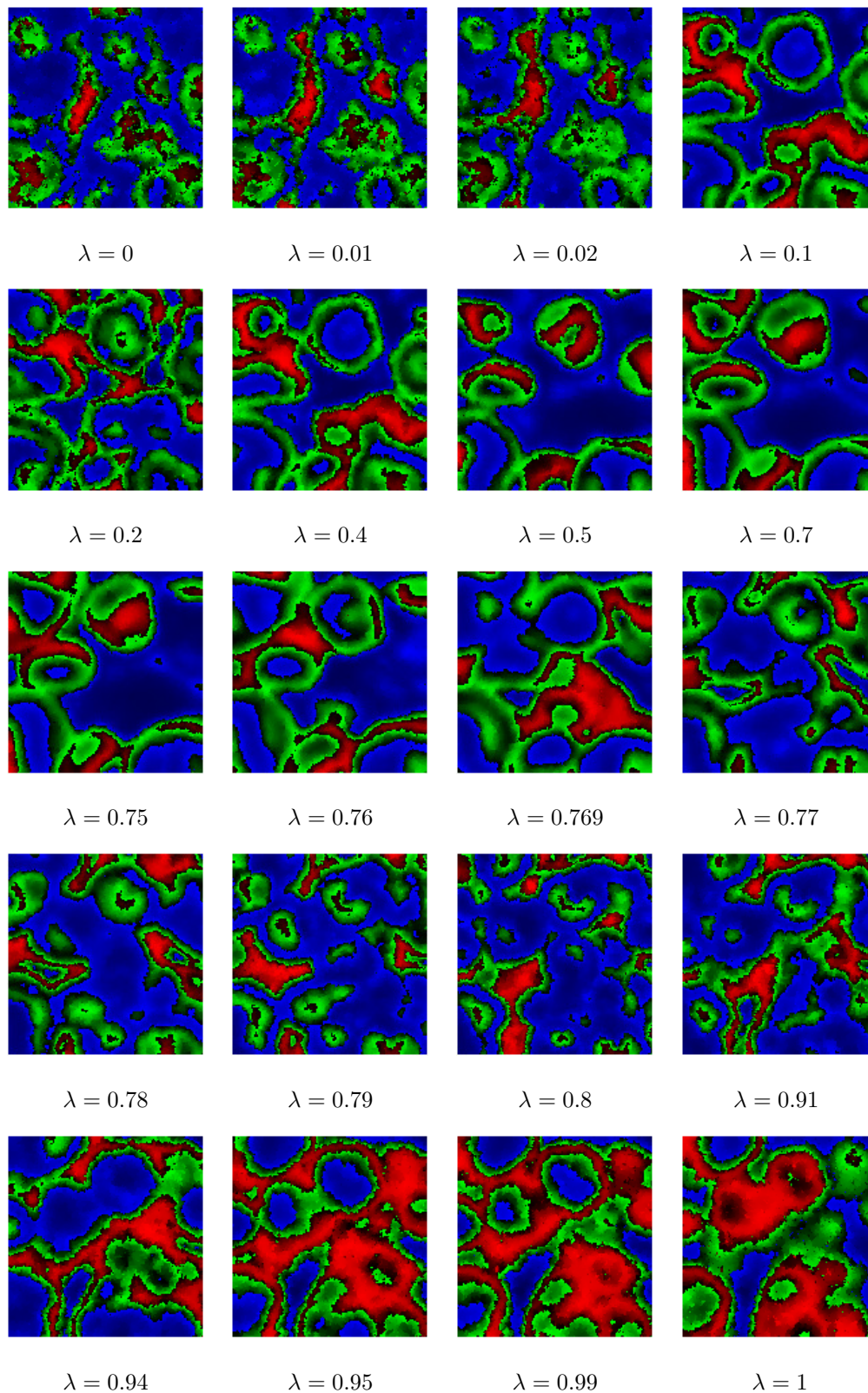
30

Figure 16: Nonlinear waves for the state $x_{i,j}$ in the *double-layer* autonomous Lotka-Volterra CNN (68). Here, λ is the homotopy parameter. These figures are not static, but dynamic (always changing) images at the instant of $t = 500$. The initial condition $v_{i,j}(0)$ is given by the random noise image in Fig. 3. The step size h of the Euler method is set to 0.002.

4   Conclusion

We have studied the complex nonlinear waves and the bifurcation phenomena of the autonomous CNNs with the two layers of memristor coupling, using the homotopy method. Furthermore, we have shown that this method gives the new approach to the analysis of the complex nonlinear waves in the autonomous CNNs with double layers. In this paper, we used the Euler method for solving the autonomous CNN equations. In order to get more accurate results, we may need high accuracy numerical methods. Furthermore, we used the synchronous parallel model to obtain the solutions of the autonomous CNN equations. If we use the sequential model, then we may obtain similar but little different results.

References

[1] Itoh, M.(2019) Nonlinear Waves in Two-Dimensional Autonomous Cellular Neural Networks Coupled by Memristors, viXra:1912.0197 [Category: Mathematical Physics],

[2] Chua L.O., Hasler M., Moschytz G.S., and Neirynsk J. (1995) Autonomous Cellular Neural Networks: A Unified Paradigm for Pattern Formation and Active Wave Propagation, *IEEE Trans. CAS-I*, **42**(10), 559-577.

[3] Madan, R.N. (1993) *Chua's Circuit: A Paradigm for Chaos* (World Scientific, Singapore).

[4] Hirsch, M.W., Smale, S., and Devaney, R.L. (2003) *Differential Equations, Dynamical Systems, and an Introduction to Chaos, Second Edition* (Elsevier Academic Press, Amsterdam).

[5] Chua, L. (2015) Everything You Wish to Know About Memristors But Are Afraid to Ask, *Radioengineering* **24**(2), 319-368.

[6] Itoh, M.(2019b) Memristor Circuit Equations with Periodic Forcing, viXra:1902.0345 [Category: Mathematical Physics].